Title: Enhanced CO_2 photocatalytic reduction on alkali-decorated graphitic carbon nitride

Authors: Zhuxing Sun, Julia Melisande Theresa Agatha Fischer, Qian Li, Jing Hu, Qijun Tang, Haiqiang Wang, Zhongbiao Wu, Marlies Hankel, Debra J. Searles, Lianzhou Wang

PII: S0926-3373(17)30483-6
DOI: http://dx.doi.org/doi:10.1016/j.apcatb.2017.05.064
Reference: APCATB 15706

To appear in: *Applied Catalysis B: Environmental*

Received date: 16-2-2017
Revised date: 11-5-2017
Accepted date: 22-5-2017

Please cite this article as: Zhuxing Sun, Julia Melisande Theresa Agatha Fischer, Qian Li, Jing Hu, Qijun Tang, Haiqiang Wang, Zhongbiao Wu, Marlies Hankel, Debra J.Searles, Lianzhou Wang, Enhanced CO2 photocatalytic reduction on alkali-decorated graphitic carbon nitride, Applied Catalysis B, Environmentalhttp://dx.doi.org/10.1016/j.apcatb.2017.05.064

Enhanced CO_2 photocatalytic reduction on alkali-decorated graphitic carbon nitride

Zhuxing Sun [a,b,c,†], Julia Melisande Theresa Agatha Fischer [d,†], Qian Li [a,b], Jing Hu [a,b], Qijun Tang [a,b], Haiqiang Wang [a,b*], Zhongbiao Wu [a,b], Marlies Hankel [d], Debra J. Searles [d,e], Lianzhou Wang [c*]

[a] Key Laboratory of Environment Remediation and Ecological Health, Ministry of Education, College of Environmental & Resources Science, Zhejiang University, Hangzhou 310058, P.R. China

[b] Zhejiang Provincial Engineering Research Center of Industrial Boiler & Furnace Flue Gas Pollution Control, Hangzhou, 311202, P. R. China

[c] Nanomaterials Centre, School of Chemical Engineering and Australian Institute for Bioengineering and Nanotechnology, The University of Queensland, Brisbane, QLD 4072, Australia

[d] Australian Institute of Bioengineering & Nanotechnology, The University of Queensland, QLD 4072, Australia

[e] School of Chemistry and Molecular Biosciences, The University of Queensland, QLD 4072, Australia

[†] These authors contributed equally.

Graphical Abstract

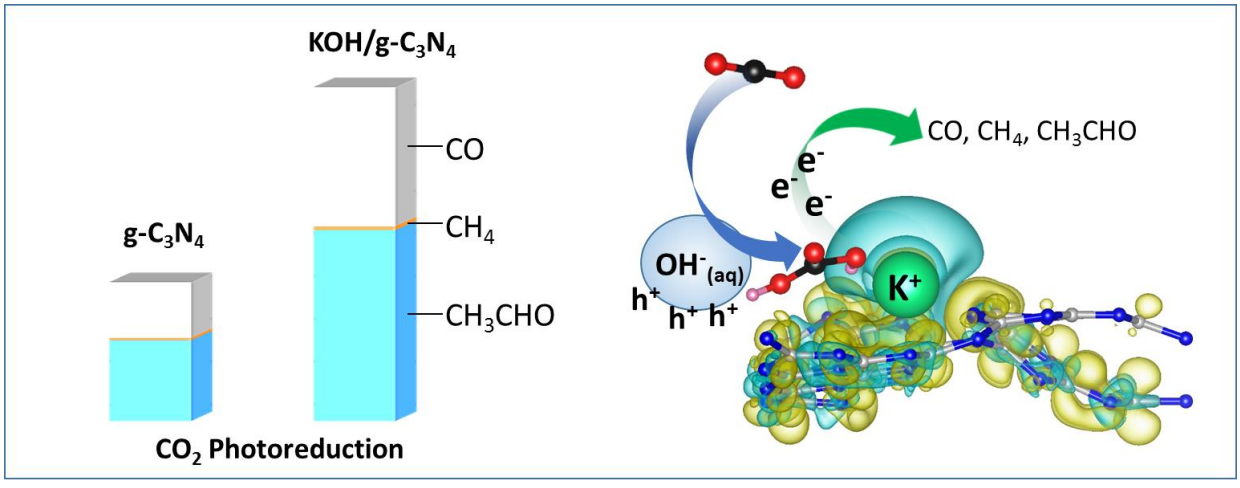

* Corresponding authors:

(H. Wang) E-mail: haiqiangwang@zju.edu.cn; Tel. / Fax: +86-571-87953088.

(L.Wang) E-mail: l.wang@uq.edu.au; Tel: + 61 7 33654218 Fax: + 61 7 33654199

Highlights

- 3-fold enhancement in CO_2 photocatalytic reduction is achieved on KOH-decorated g-C_3N_4.
- A thin layer of electrolyte is expected to form due to the easy deliquescence of KOH
- OH^- functions as hole accepters to improve the separation and utilization of charges
- OH^- also keeps a dynamically stable amount of the main species to be reduced
- K^+ in KOH enhanced the binding of H_2CO_3 on g-C_3N_4 in a greater extent than Na^+ in NaOH

Abstract

In this work, visible-light photocatalytic reduction performance of carbon dioxide (CO_2) on graphitic carbon nitride (g-C_3N_4) was significantly promoted by the decoration of potassium hydroxide (KOH) on g-C_3N_4. More importantly, the role of KOH was thoroughly discussed via various characterizations, control experiments and density functional theory (DFT) calculations. It was found that KOH decoration did not result in any significant difference regards to the morphologies, elemental states, BET surface areas and light adsorption of g-C_3N_4 except a drastically enhanced CO_2 adsorption capacity. The promotion effect of KOH on g-C_3N_4 was mainly contributed by the hydroxide ion (OH^-) functioning as both a hole accepter and a driving force to keep a dynamically stable amount of H_2CO_3 (probably the major form of CO_2 to be reduced) on the surface of the catalyst. Moreover, the different extents of influence of NaOH and KOH on g-C_3N_4 were revealed and further explained using computational results. This study supplements current understanding on alkali-promoted photocatalytic processes and provides new insights into the mechanism of CO_2 photocatalytic reduction.

Keywords: CO_2 conversion; photocatalysis; g-C_3N_4; alkali; DFT calculations

1. Introduction

Photocatalytic reduction of carbon dioxide (CO_2) into fuel (methane, methanol, carbon monoxide etc.) with water as reducing agent is a green technology that aims to mimic the photosynthesis process in nature and has attracted increasing attention in the past few decades. [1-7] The major challenge and focus of studies in this area is the development of an efficient, stable and cost-effective photocatalyst. Over the past four decades, various semiconductor photocatalyts including metal oxide (TiO_2, [8] Cu_2O, [9] CeO_2 [10, 11]); oxysalt ($KTaO_3$, [12] Bi_2WO_6 [13] etc.), metal chalcogenides (ZnS, [14] Bi_2S_3, [15] etc.), and non-metal materials (graphene oxide, [16] carbon nitride, [17] etc.) have been studied for photocatalytic conversion of CO_2. Among them, graphitic carbon nitride (g-C_3N_4), has gained tremendous attention recently as an easily-obtained, low-cost and visible-light-responsive

non-metal semiconductor photocatalyst that shows great stability and non-toxicity. [7, 18-25]

There have been several pioneering reports on the use of g-C_3N_4 for CO_2 photocatalytic reduction. [20, 21] The CO_2 photocatalytic reduction on g-C_3N_4 was successfully enhanced by forming heterojunctions or Z-scheme structures with other semiconductors such as In_2O_3, [26] $NaNbO_3$, [27] Bi_2WO_6, [28] $BiVO_4$, [29] Ag_3PO_4, [30] BiOI, [31] $LaPO_4$, [32] ZnO, [33, 34] CeO [35] and AgBr/graphene. [36] These improvements were mainly due to the promotion of separation and transfer of photo-generated electrons and holes, addressing one of the major drawbacks of g-C_3N_4. Another major problem in use of g-C_3N_4 for photocatalytic CO_2 reduction is its limited ability to adsorb/activate CO_2, although this issue is usually less emphasized. Amine functionalization [37] and UIO66 [38] (a type of metal organic framework) have been applied to enhance CO_2 adsorption on g-C_3N_4 in order to achieve superior CO_2 conversion. This suggests that increasing the amount of adsorbed CO_2 is an effective method to enhance CO_2 photocatalytic reduction on g-C_3N_4.

Recently, the alkaline earth metal oxide, MgO, [39-42] and the alkali, NaOH, [43] have been reported to be able to enhance CO_2 photocatalytic conversion on TiO_2. The positive influences were attributed to an enhanced CO_2 activation and, probably more importantly, a facilitated oxidation process. However, a detailed understanding of the overall mechanism is lacking.

In this work, KOH was decorated on g-C_3N_4 and a 3-fold enhancement in production of carbon monoxide (CO), methane (CH_4) and acetaldehyde (CH_3CHO) from photocatalytic reduction of CO_2 was observed. To understand the role of KOH, detailed characterizations, control experiments, and DFT calculations were carried out. The difference between KOH and NaOH were also discussed to emphasize the important influence of the cations on the photocatalytic reduction performance.

2. Experimental

2.1 Sample preparation

All chemicals were analytically pure and used without further treatment. Graphitic carbon nitride (g-C_3N_4) was synthesized by heating 30 g of urea in a 100 ml crucible with a cover in static air at 550 °C for 2 h with a ramping rate of 10 °C min^{-1}. We refer to this sample as CN.

KOH and NaOH were deposited on g-C_3N_4 by simply impregnating 0.6 g of g-C_3N_4 in aqueous solution with various quantities of KOH (0.05, 0.1, 0.25, 0.5, 1.0 wt%) or NaOH (0.5, 1.0, 2.0, 3.0 wt%). The suspensions were sonicated and stirred to fully disperse the g-C_3N_4 and then dried in a rotary evaporator. Finally, the dried sample was recollected and ready

for use. The samples were denoted as xKOH-CN (x = 0.05, 0.1, 0.25, 0.5, 1.0) and yNaOH-CN (y = 0.5, 1.0, 2.0, 3.0). KCl, $KHCO_3$ and K_2CO_3 patched g-C_3N_4 samples were also prepared in the same way.

2.2 Characterization methods

X-ray powder diffraction (XRD) patterns were recorded on an X-ray diffractometer (Model D/max RA, Japan) with Cu Kα irradiation. Fourier transform infrared (FTIR) spectra were obtained on an FTIR spectrometer (Bruker Alpha, Germany) equipped with a deuterated triglycine sulfate (DTGS) detector using sample discs prepared with dried KBr. X-ray photoelectron spectroscopy (XPS: Thermo ESCALAB 250Xi, USA) measurements were performed with a monochromatized Al Kα source (150 W, 500 μm, hv =1486.6 eV). The carbon 1s line (284.8 eV) was used as the reference to calibrate the binding energies. Field emission scanning electron microscope (FE-SEM: Hitacha SU8020, Japan) and transmission electron microscope (TEM, Fei F20, USA, Voltage: 200KV) were used to study the morphology of the samples. The Brunauer-Emmett-Teller (BET) specific surface area was calculated from the multipoint BET method on a physisorption analyzer (JW-BK 132F, Beijing JWGB Sci & Tech Co., China). The UV-Vis diffuse reflection spectra (UV-Vis DRS) were obtained on an UV-Vis spectrophotometer (TU-1901, China) equipped with an integrating sphere assembly and $BaSO_4$ was used as the reflectance. The photoluminescence spectra were measured with a fluorescence spectrophotometer (RAMANLOG 6, USA) using 420 nm lasers as excitation source. The photocurrent of the samples at different pH was measured on an electrochemical workstation (CHI 660E, China) with 1.5 M Na_2SO_4 as the electrolyte. The pH was tuned by addition of KOH or NaOH. CO_2 adsorption tests were carried out on a thermo gravimetric analysis instrument (TGA, SDT Q600 V8.2 Build 100). The samples were pretreated with flowing He at 120 °C for 2 h and exposed to CO_2 at 50 °C. The changes in weights during the process were recorded to value their CO_2 adsorption capacities.

2.3 CO_2 photocatalytic reduction experiment

CO_2 photocatalytic conversion in the presence of H_2O was conducted in a homemade stainless-steel-made reactor with a quartz window on the top. The system was operated in a continuous-flow mode. For each test, 40 mg of catalyst was evenly dispersed at the bottom of the reactor. A 300 W Xeon lamp (PLS-SXE300UV, Beijing Trust-tech Co. Ltd, China) with a light filter was used to obtain visible light with wavelengths larger than 420 nm. (To note, the CO_2 photocatalytic reduction experiments to compare the influence of anions in section 3.3 were conducted under irradiation of the full spectrum of the Xeon light.) After the reactor was sealed, CO_2 (99.9999%) was purged into the reactor through a water bubbler, delivering a gas mixture of CO_2 and H_2O, at 120 ml·min^{-1} for 1 h in order to remove any

impurity gases. Then the flow was maintained at 3.0 ml·min^{-1} for another 1 h to stabilize the system before the irradiation source was turned on. During the reaction, gaseous products in the reactor effluent were analyzed at certain time intervals using a calibrated gas chromatography (Agilent 7890A, USA) which was equipped with two flame ionization detectors (FID) and a thermal conductivity detector (TCD). The accumulated yields of the products were obtained by integrating the production rate over time. The samples after reaction were collected to check if there are any products attached on the surface by extraction with water and subsequent detection with GC (for hydrocarbons) and ion chromatograph (for formic acid mainly). Experiments without light irradiation, using N_2 instead of CO_2 and without addition of a catalyst, were also conducted and little product could be detected, indicating that the products are from the photocatalytic reduction of CO_2. In addition, isotope tracing experiments were also conducted using $^{13}CO_2$ (99 atom% C, SIGMA-ALDRICH Co.) in a batch reactor and confirmed that the products are from CO_2 rather than from any carbon-containing contaminants.

2.4 In situ DRIFTS experiments

In situ diffuse reflectance FT-IR spectroscopy (DRIFTS) was carried out on a Nicolet 6700 spectrometer (Thermo Electron) equipped with a liquid nitrogen cooled HgCdTe (MCT) detector, a Praying Mantis DRIFTS accessory and a reaction cell (Harrick Scientific, HVC-DRP). The reaction chamber is equipped with a heater and a temperature controller as well as a sample cup in the center. There are three windows on the dome of the cell: two CaF windows for IR transmission and a quartz window allowing transmission of irradiation light from a 300W Xe lamp (PLS-SXE300UV, Beijing Trust-tech Co. Ltd, China). The spectra recorded were displayed in absorbance units and acquired with a resolution of 4 cm^{-1}, using 32 scans.

After the sample was loaded in the reaction cell, the cell was purged with helium (He) at 30 ml min^{-1} at 200 °C for 1h to eliminate any absorbed gas on the surface of the sample and any impurity gases in the chamber. Then the cell was cooled down to 50 °C and the background spectrum was collected. Subsequently, a CO_2/H_2O mixture, delivered by passing CO_2 through a water bubbler at 3 ml min^{-1}, was introduced to allow absorption saturation. IR spectra were recorded as a function of time (0-60 min). To eliminate any physisorbed species, the system was purged with He again for 30 min. Subsequently, the light was turned on and the system was irradiated for 120 min while the time-resolved IR spectra were collected to investigate chemical changes on the sample surface.

2.5 Computational Methods

All calculations were performed with Vienna Ab Initio Simulation Package (VASP) [44] with periodic boundary conditions and projector-augmented wave (PAW) [44]. The generalized gradient approximation (GGA) with the Perdew-Burke-Ernzerhof (PBE) functional [45] and dispersion correction by Grimme (DFT-D2) [46] were used to describe the electronic structure. For the 2×2 unit cell, the Brillouin zone was sampled by a 3×3×1 k-point mesh and a cutoff energy of 500 eV was used. The vacuum slap between two layers was set to 20 Å.

A positive binding energy (E_{bind}) indicates stable adsorption at 0 K, and was calculated by the difference between the total energies of the surface with adsorbates (E_{SF+mol}) and energies of the two separate systems (the surface E_{SF} and of the molecule E_{mol}):

$$E_{bind} = -(E_{SF+mol} - E_{SF} - E_{mol}) \quad (1)$$

There are number of stoichiometrically equivalent structures of g-C_3N_4 and here we consider the structure which comprises tri-s-triazine (also referred to as heptazine) units connect through graphitic nitrogen atoms to form a 2D sheet. Details on the preparations of the corrugated sheets, can be found in the supporting information. To model the g-C_3N_4 surface, we used a 2×2 supercell of g-C_6N_8 [47], with an optimized lattice constant of 13.59 Å for the corrugated sheets. Furthermore, to include the –NH bond, one of the tri-*s*-triazine units of g-C_6N_8-units was replaced by three hydrogen atoms, to saturate the three nitrogen dangling bonds. Both of these systems are shown in Fig. 1. The corrugation of the sheet was separately calculated and the optimized lattice constant for the –NH containing system was determined to be 13.83 Å.

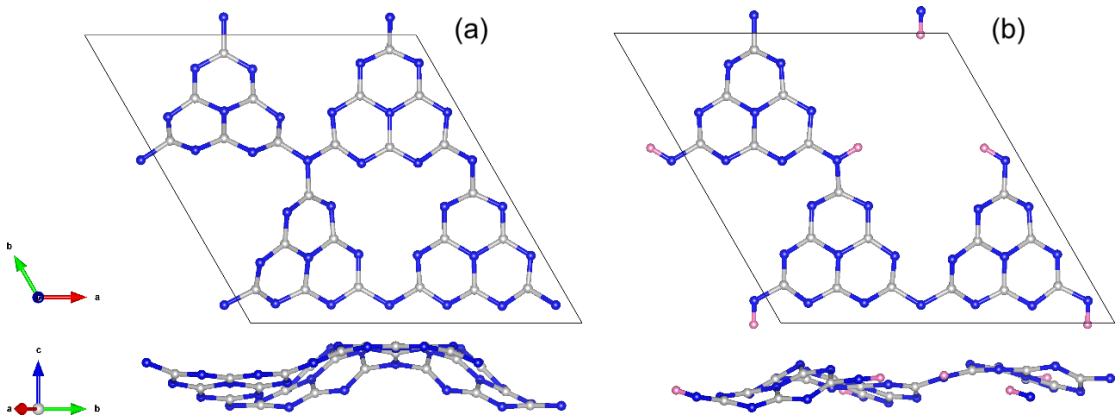

Fig. 1 Unit cell for g-C_3N_4 (a) and –NH containing g-C_3N_4 (b). (Grey – carbon atoms, blue – nitrogen atoms and pink – hydrogen atoms.)

3. Results and Discussion

3.1 Physical and optical properties

The XRD patterns of CN, 0.1KOH-CN and 1.0KOH-CN are presented in Fig. 2a. All the samples show the characteristic diffraction peaks of g-C_3N_4 at 2θ = 12.9° and 2θ = 27.5°. The strongest peak at 2θ = 27.5° is indexed to the [002] plane with d = 0.326 nm, a characteristic interlayer spacing of CN aromatic units. The peak at 2θ = 12.9° is ascribed to the in-plane structural packing motif of tri-s-triazine units. [19] No new peaks or peak shifts are observed after KOH decoration. However, interestingly, the peak intensity increases with the amount of KOH. As all the samples were tested under the same conditions, the difference in peak intensity could not be attributed to measurement errors. This suggests that the impregnation of g-C_3N_4 in KOH solution and the following evaporation process could have helped the g-C_3N_4 form structures with enhanced ordering. Fig. 2b presents the FTIR spectra of the samples. All the samples show adsorption in the same ranges, i.e. 810 cm^{-1} for the breathing mode of the tri-*s*-triazine units, 1100~1650 cm^{-1} for typical stretching modes of heterocycles of carbon and nitrogen and broad adsorption at 2700~3600 cm^{-1} from stretching vibration modes of –NH [48] without much difference, indicating that the loading of KOH cannot change the main functional groups of g-C_3N_4. And, due to the low amount of KOH, the FTIR peaks of KOH could be too minor to be recognizable.

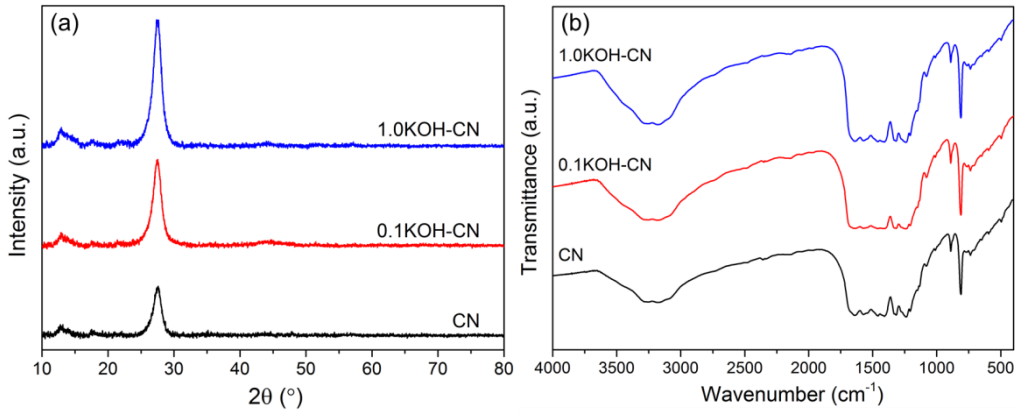

Fig. 2 XRD patterns (a) and FTIR spectra (b) of CN, 0.1KOH-CN and 1.0KOH-CN.

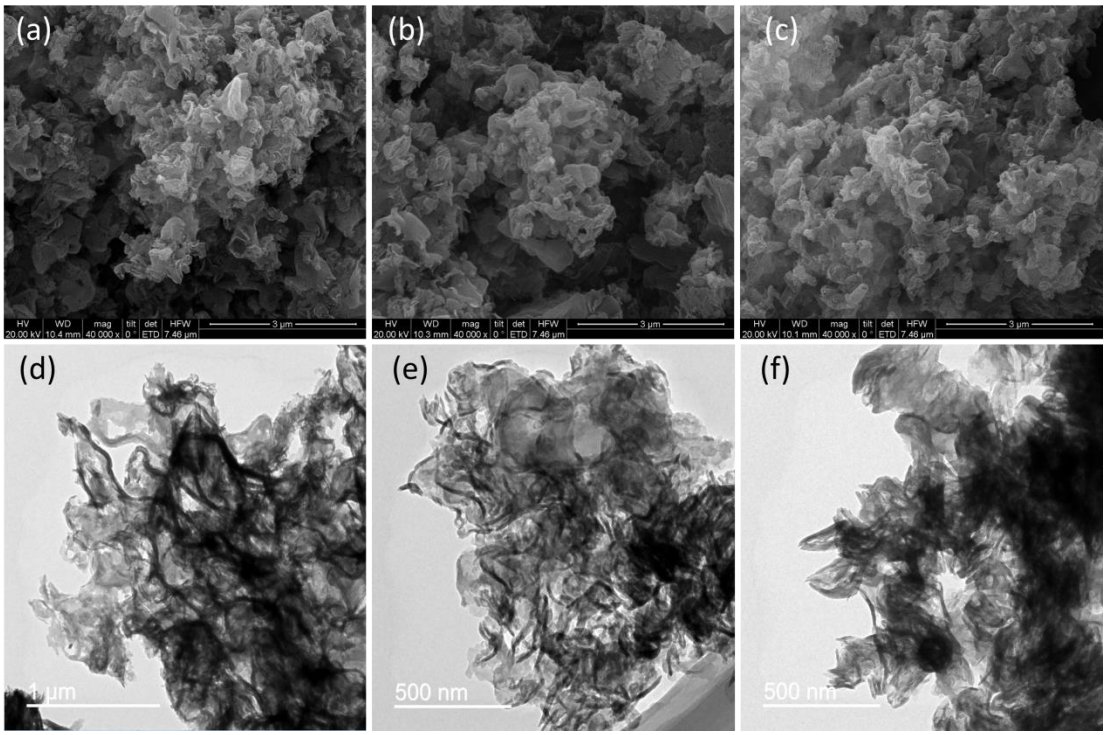

Fig. 3 SEM (a, b, c) and TEM images (d, e, f) of CN (a, d), 0.1KOH-CN (b, e) and 1.0 KOH-CN (c, f).

The morphology and microstructure of the samples were investigated by scanning electron microscope (SEM) and transmission electron microscope (TEM), as shown in Fig. 3. No apparent difference could be observed between CN and KOH-loaded CN. All the samples show morphologies of curved porous sheets stacking together as commonly reported for g-C_3N_4 synthesized from urea. [49-52] In addition, the BET surface areas calculated from N_2 adsorption-desorption tests of the unmodified and all the KOH-decorated g-C_3N_4 are very close to each other, as listed in Table 1. These suggest that the preparation processes have

little influence to the macrostructure of g-C_3N_4 and the limited amount of KOH should just have been deposited on the surface of g-C_3N_4.

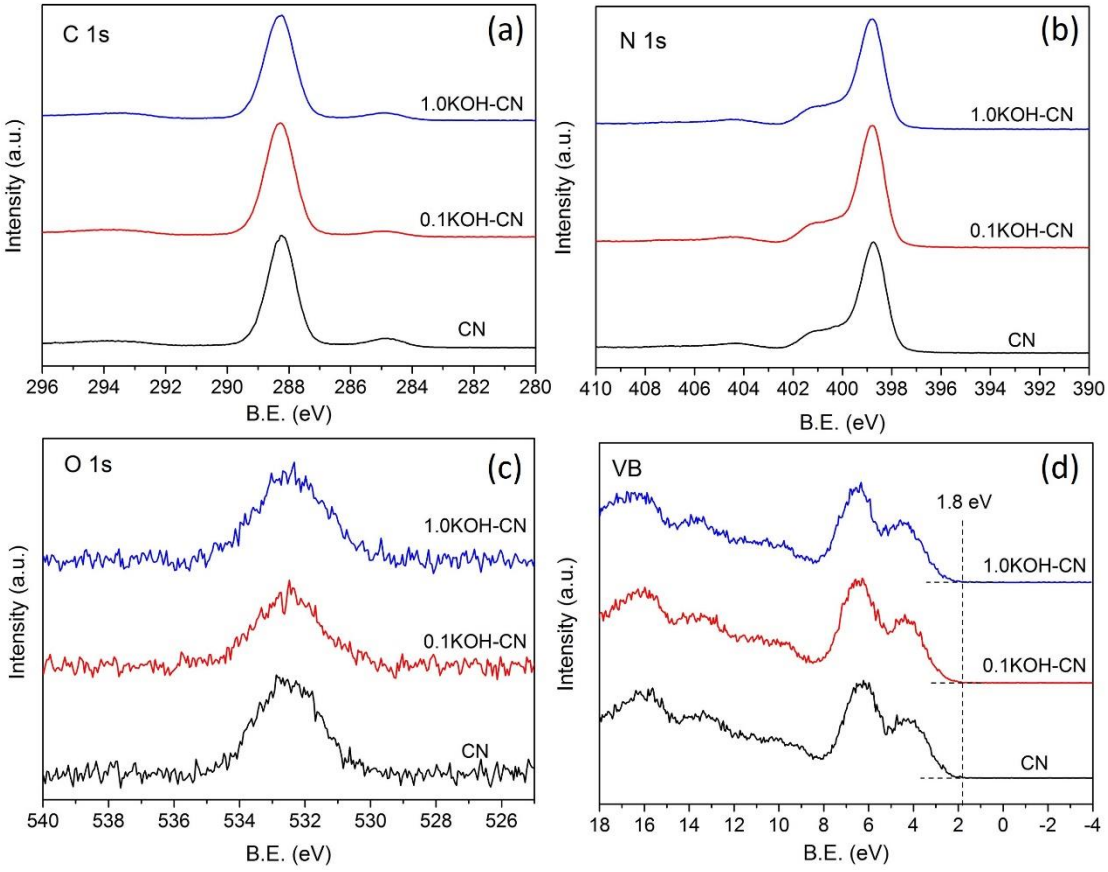

Fig. 4 C1s (a), N1s (b), O1s (c) and VB (d) XPS spectra of CN, 0.1KOH-CN and 1.0KOH-CN.

Subsequently, X-ray photoelectron spectroscopy (XPS) measurements were carried out to analyze the chemical states of the elements in the samples before and after KOH loading. Fig. 4 exhibits C 1s, N 1s, O 1s and VB XPS spectra of CN, 0.1KOH-CN and 1.0KOH-CN. The states of carbon, nitrogen and oxygen as well as the VB location changed little before and after KOH loading. The binding energy of K 2p is 292-295 eV but no peaks in this range are visible in the XPS spectra of 0.1KOH-CN and 1.0KOH-CN due to the low content of KOH in these samples.

The amount of oxygen in CN, 0.1KOH-CN and 1.0KOH-CN are estimated to be 5.6 at%, 8.1 at% and 12.1 at%, respectively based on peak areas in the XPS survey spectra. The oxygen could mainly consist of residual oxygen from the polymerization process of urea [49] and the oxygen from KOH. As the amount of the former form of oxygen should be consistent in all samples, the increased amount of oxygen is expected to be from the increased amount of deposited KOH. Besides, a peak due to K can be observed in the energy dispersive X-ray

(EDX) test in SEM of the 1.0KOH-CN sample (Fig. 5) with the content estimated to be around 0.8 wt% (~1.48 at%), suggesting the successful decoration of KOH on the surface of g-C_3N_4.

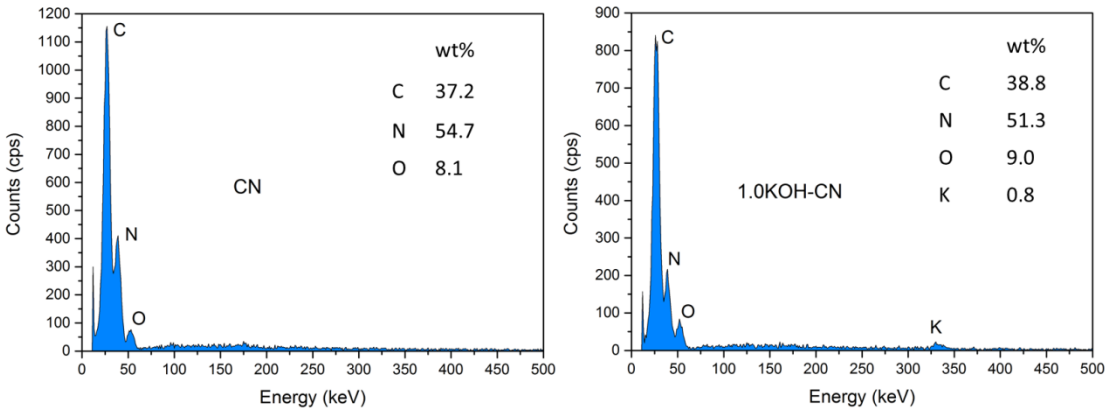

Fig. 5 SEM-EDX spectra of CN and 1.0KOH-CN.

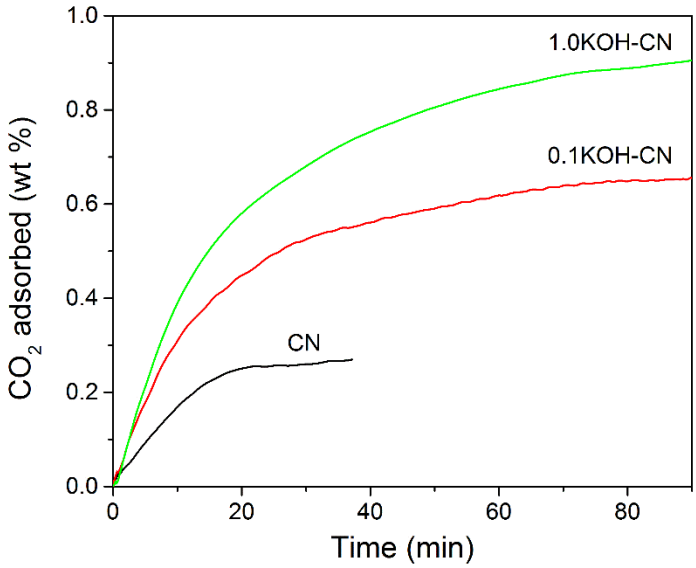

Fig. 6 CO_2 absorption curves of CN, 0.1KOH-CN and 1.0KOH-CN at 50 °C.

CO_2 adsorption at 50 °C (Fig. 6) further verifies the successful loading of KOH on the sample surface. While CN only adsorbs 0.28 wt% CO_2, 0.65 wt% CO_2 is adsorbed on 0.1KOH-CN and a further increase (0.9 wt%) is observed on 1.0 KOH-CN. As mentioned above, CN, 0.1KOH-CN and 1.0KOH-CN possess similar BET surface areas. The KOH deposited on g-C_3N_4 is expected to be the only cause for the enhanced CO_2 adsorption.

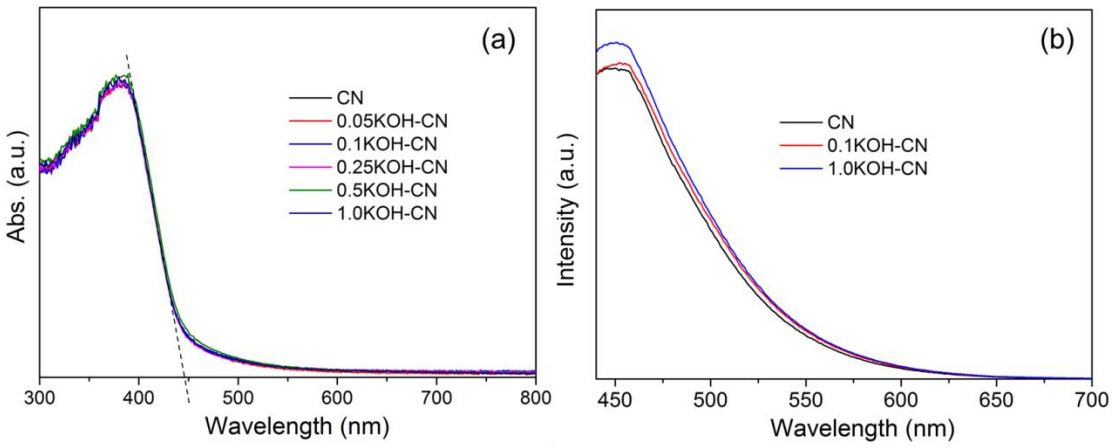

Fig. 7 UV-vis diffraction spectra of CN and CN with various KOH loading amount (a) and PL spectra of CN, 0.1KOH-CN and 1.0KOH-CN (b).

In terms of optical properties, KOH exerted little influence on the light absorption of g-C_3N_4. As demonstrated in Fig. 7a, all the g-C_3N_4 samples without or with different amount of KOH show the same light adsorption ranges with the absorption edge at around 450 nm. Fig. 7b gives the photoluminescence (PL) spectra of CN, 0.1KOH-CN and 1.0KOH-CN. The peak locations of the three samples are alike. A small increase in intensity is observed as the KOH loading amount increases. This suggests that the addition of KOH slightly increases the recombination rate of photo-generated electrons and holes. However, this effect is too small for 0.1KOH-CN to cause any possible influence to the photocatalytic activity of g-C_3N_4.

3.2 CO_2 photocatalytic reduction on KOH-loaded g-C_3N_4

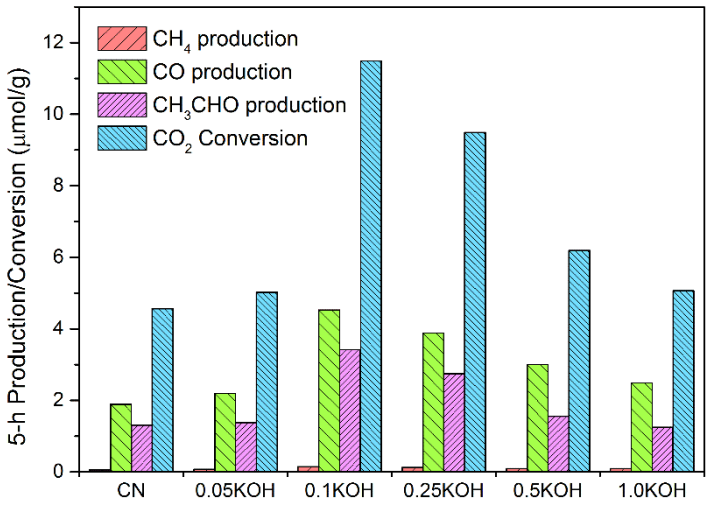

Fig. 8 5-h production of CO, CH_4 and CH_3CHO and conversion of CO_2 over CN and CN decorated with different amount of KOH (denoted as xKOH, x = 0.05, 0.1, 0.25, 0.5 and 1.0) in photocatalytic CO_2 reduction under visible light irradiation ($\lambda > 420$ nm)

The 5-h productions in CO_2 photocatalytic reduction under visible light (λ > 420 nm) using CN and its corresponding samples with KOH decoration as photocatalyst are presented in Fig. 8 while the time-dependent data is provided in Fig S1 (supporting information). The products detected consist of CO, CH_4 and CH_3CHO and the detailed amounts of the compounds produced as well as the contributions of the whole CO_2 converted are listed in Table S1 (supporting information). Liquid products such as formaldehyde, methanol and ethanol were not detected in the current reaction system. As shown in Fig.8, the productions of all the products increase with the addition of 0.05 wt% KOH. When 0.1 wt% KOH is used, the productions increase greatly and became about 3 times larger than those of CN. However, an excessive amount of KOH (0.25, 0.5, 1.0 wt%) does not result in a further increase in the production of CO, CH_4 or CH_3CHO but lowers the productions as it goes on increasing.

3.3 Effect of anions

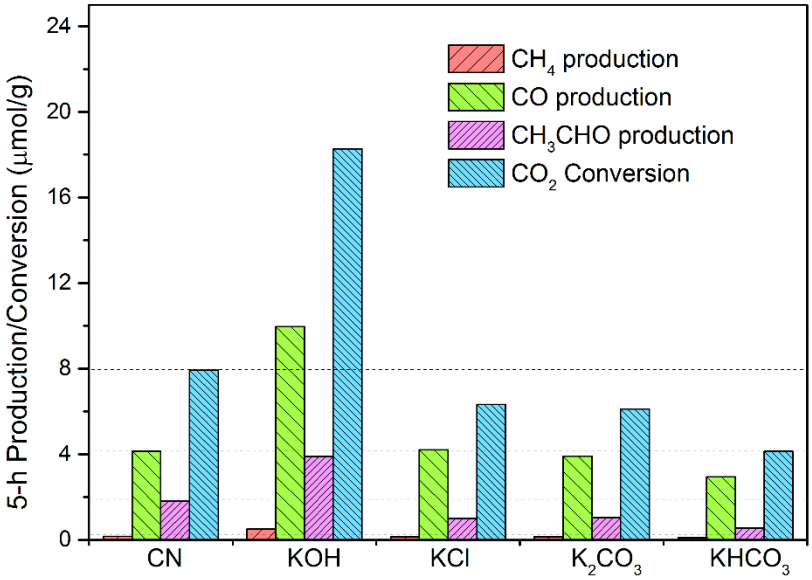

Fig. 9 5-h production of CO, CH_4 and CH_3CHO and conversion of CO_2 over CN and CN loaded with KOH, KCl, K_2CO_3 and $KHCO_3$ respectively in photocatalytic CO_2 reduction under irradiation of Xeon lamp.

To clarify the role of KOH in enhancing the CO_2 reduction performance, we considered firstly if the cation K^+ could be responsible for the increase in CO_2 reduction and secondly whether the bicarbonates and/or carbonates (i.e. $KHCO_3$ and K_2CO_3) that formed from reaction between KOH and CO_2 would participate in the catalytic process and facilitate the reactions. Therefore, CO_2 photocatalytic reduction performance of g-C_3N_4 decorated with KOH (0.1 wt%), KCl (0.13 wt%), K_2CO_3 (0.12 wt%) and $KHCO_3$ (0.18 wt%), respectively were further compared. The atomic ratio of K in each sample was kept the same. The results are

illustrated in Fig. 9 and Fig. S2. Compared to the pristine CN, the samples loaded with KCl, K_2CO_3 and $KHCO_3$ show no improvement in CO or CH_4 production and the yields of CH_3CHO over them even decrease obviously. The results indicate that K^+ alone is not able to promote the reactions, and that neither $KHCO_3$ nor K_2CO_3 would promote the conversion of CO_2.

When focusing on the first 100-min productions of CO and CH_4, as shown in Fig. S3 (d) and (e), it is found that $KHCO_3$-CN shows superior CH_4 production to that of CN in the first 100 min. However, the influence does not last, and final productions in 5 h over $KHCO_3$-CN are poor. This suggests that HCO_3^- could be an adsorbed species that contributed to CH_4 formation, but could not influence the CO_2 adsorption or reduction significantly. All of these suggest that the existence of OH^- along with its high alkalinity is indispensable for the enhancement in CO_2 photocatalytic reduction with KOH-CN.

3.4 Effect of cations

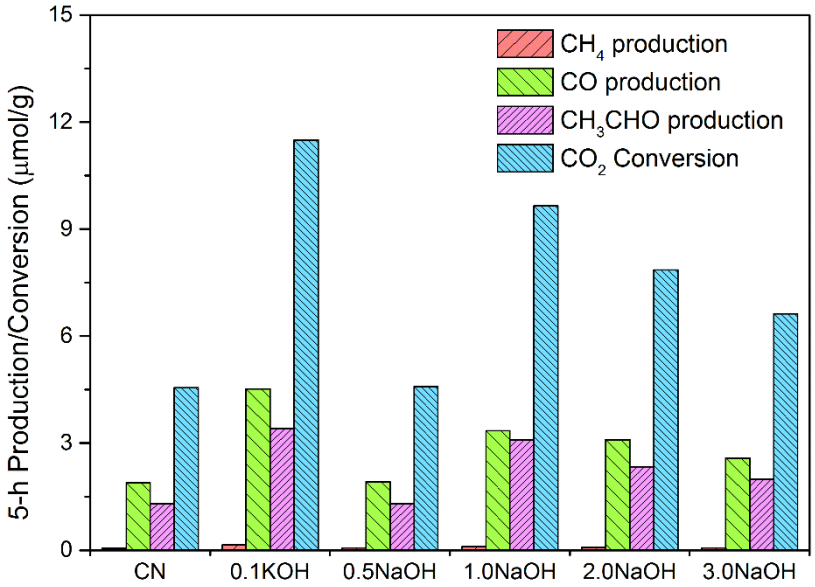

Fig. 10 5-h production of CO, CH_4 and CH_3CHO and conversion of CO_2 over Cn decorated with different amount of NaOH (denoted as xNaOH-CN, x = 0.5, 1.0, 2.0 and 3.0) in photocatalytic CO_2 reduction under visible light irradiation ($\lambda > 420$ nm) compared with 0.1KOH-CN (denoted as 0.1KOH) and CN.

Fig. 10 and Fig. S3 exhibit the accumulated and time-resolved product yields respectively in CO_2 photocatalytic reduction over g-C_3N_4 loaded with different amounts of NaOH with a comparison with those of CN and 0.1KOH-CN. NaOH-CN presents enhanced activity compared to CN as well. However, the optimal loading amount of NaOH is 1.0 wt%, which is 10 times larger than that of KOH. In addition, although the optimal CH_3CHO yields on 1.0NaOH-CN and 0.1KOH-CN are very close, the production of CO and CH_4 over the best

KOH-CN is about 1.5 times that of the best NaOH-CN. This implies that the characteristics of the cation are also important to determine the influence of the alkali on the photocatalyst ($g\text{-}C_3N_4$).

3.5 Discussion on the roles of KOH

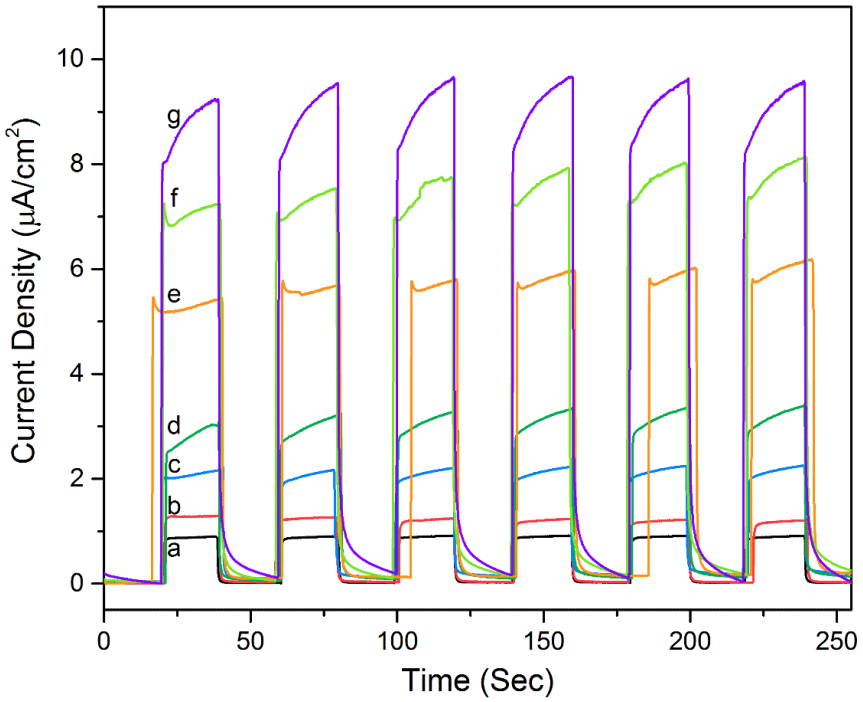

Fig. 11 Photocurrent of $g\text{-}C_3N_4$ at different pH values (the pH of a-f are tuned by KOH: a -pH 8.64; b-pH 9.55; c-pH 11.29; d-pH 12.35; e-pH 13.09; f-pH 13.59; the pH of g is tuned by NaOH: g-pH 13.58).

Firstly, it is possible that OH^- on $g\text{-}C_3N_4$ functions as a hole scavenger and helps enhance the separation of photo-generated charges and thus the CO_2 conversion efficiency. [43, 53] To verify this point, photocurrents of urea-polymerized $g\text{-}C_3N_4$ at Na_2SO_4 solution of different pH values tuned by KOH or NaOH were obtained, as presented in Fig. 11. The photocurrent increases significantly as the pH value rises, suggesting OH^- can accept the photo-generated holes and suppress the recombination rate of the photo-excited charges. However, it is also found that the photocurrent of $g\text{-}C_3N_4$ in Na_2SO_4 solution with a pH of 13.59 adjusted by KOH is lower than that in Na_2SO_4 solution with a pH of 13.58 adjusted by NaOH. If the improvement in CO_2 photocatalytic reduction is predominantly due to the role of OH^- as a hole acceptor, the performance of KOH-CN and NaOH-CN should be close to each other, with NaOH possibly showing a greater promotion. But this is in contradiction with our observation that NaOH-CN has a lower enhancement in CO_2 reduction and a 10 times higher

optimal loading than that of KOH-CN. Therefore, it can be deduced that there should be other factor(s) influencing the performance of the alkali-decorated g-C_3N_4.

Secondly, studies on the photochemical reduction [2, 8, 54, 55] of CO_2 adsorbed in water, suggest that H_2CO_3 and dissolved CO_2 are highly likely to be the reactive species. As KOH and NaOH are deliquescent, a thin layer of alkaline electrolyte is expected to form on the surface of alkali decorated g-C_3N_4 in the present water vapor and CO_2. [52] The equilibria of CO_2 in water and basic solution are:

$$CO_2 + H_2O \rightleftarrows H_2CO_3 \quad (2)$$

$$H_2CO_3 + OH^- \rightleftarrows HCO_3^- + H_2O \quad (3)$$

$$HCO_3^- + OH^- \rightleftarrows CO_3^{2-} + H_2O \quad (4)$$

In deionized water, equation (2) is dominant with dissolved CO_2 being the main carbon-containing species present. As the pH increases, the deprotonated forms of H_2CO_3 are more likely to be present. Since the addition of HCO_3^- and CO_3^{2-} showed little improvement in the catalytic performance, it is supposed that the main carbon-containing species involved in the alkali-enhanced reduction are H_2CO_3 and dissolved CO_2. Besides, a recent work [55] studied the change of carbon species in various electrolytes after bubbling CO_2 and found that after bubbling with CO_2, the ratio of H_2CO_3 (i.e. H_2CO_3 and CO_2) to the total carbon-species (i.e. H_2CO_3, CO_2, HCO_3^- and CO_3^{2-}) in a low initial concentration of KOH (0.1M) was higher than that in $KHCO_3$ (0.1 M). But this value would decrease dramatically if the concentration of KOH increased. In light of this, a low amount of OH^-, as on our KOH decorated sample, may be able to keep a dynamically stable amount of H_2CO_3 in the thin layer of solution on the catalyst's surface. Subsequently, the photocatalytic process with OH^- as hole scavengers would consume the stabilized H_2CO_3 before it changes to its HCO_3^- or CO_3^{2-}. Thus, a formation-consumption cycle of H_2CO_3 could be realized. In other words, a cycle of H_2CO_3 generation, photocatalytic conversion and re-generation can be achieved with the relatively low amount of OH^-. However, when the concentration of OH^- is too high, it will result in formation of CO_3^{2-} as the major species, leaving little H_2CO_3. Besides, a larger amount of alkali on the photocatalyst surface would also inhibit the transfer of photo-exited charges from g-C_3N_4. [55]

With regard to the initial enhancement of CH_4 production with $KHCO_3$-CN observed in Fig. S3, it could be explained by the fact that in the thin layer of electrolyte for the deliquescing of $KHCO_3$, HCO_3^- would coexist with H_2CO_3 through equation (3). And the H_2CO_3 would participate in the reactions when the samples are irradiated. However, $KHCO_3$ shows far less ability in adsorbing water and would form less amount of electrolyte. More essentially, the system with $KHCO_3$ lacks OH^- as both a driving force for enhanced CO_2 adsorption and a hole

acceptor. As a result, $KHCO_3$-CN does not show apparent enhancement compared to bare g-C_3N_4 over a long period.

3.6 Difference between sodium and potassium on alkali-decorated g-C_3N_4

In order to understand the difference between K (KOH) and Na (NaOH) in interacting with reducible CO_2 species on g-C_3N_4, density functional theory (DFT) calculations were performed with bare g-C_3N_4 nanosheet and g-C_3N_4 sheet with K/Na atom. The plain g-C_3N_4 nanosheet in calculation is corrugated g-C_3N_4 sheet, as exhibited in the experimental section (Fig. 1a). The most stable forms of Na/g-C_3N_4 and K/g-C_3N_4 are presented in Fig. 12. Na/g-C_3N_4 is with Na sitting most stably in the middle pore of the melon units, nearly in-plane with the g-C_3N_4 sheet for its small atomic radius, whereas the most stable site for K atom on g-C_3N_4 is on top of the whole above the g-C_3N_4 plane. Meanwhile, both Na and K are cationic on the sheet, i.e. are presenting as Na^+ and K^+ according to the charge density differences results, which will be explain in detail later.

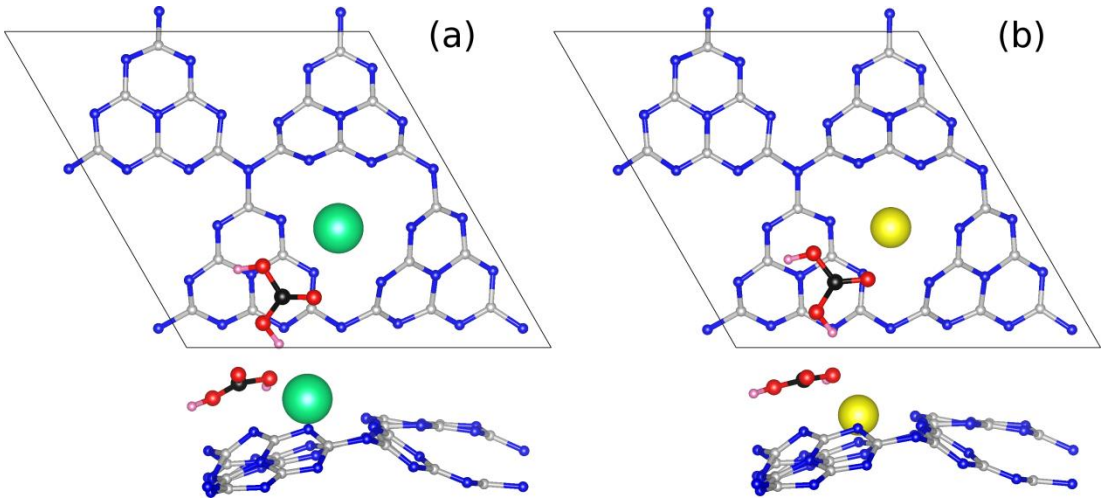

Fig. 12 Most stable adsorption sites for H_2CO_3 on g-C_3N_4 with K (a) and Na (b). (Grey, black – carbon atoms, blue – nitrogen atoms, red – oxygen atoms, pink – hydrogen atoms, green – potassium atoms and yellow – sodium atoms.)

According to our calculation results, for CO_2 adsorption on plain corrugated g-C_3N_4 sheet, the binding energy is 0.25 eV. The most stable CO_2 adsorption site is on top of the large tri-s-triazine pores and the interaction is considered to be physisorption because there is no change in the bond length of the C-O bond (1.18 Å). Neither the addition of K nor Na on g-C_3N_4 changes the binding energy of CO_2 (0.25 eV). Both K and Na share the most stable adsorption site, the pore, with CO_2 (see Fig. S4).

While substituting CO_2 with H_2CO_3, the situation becomes interestingly different. While the binding energy of H_2CO_3 on the bare g-C_3N_4 is 0.75 eV, it is 1.13 eV for K/g-C_3N_4 and 0.86

eV for Na/g-C_3N_4. This change of H_2CO_3 binding energy before and after the presence of K and Na can be regarded as an indirect indication that H_2CO_3 is the main reduced CO_2 species. And that the binding energy of H_2CO_3 on K/g-C_3N_4 was 24% larger than that on Na/g-C_3N_4 could be one of the causes that why NaOH shows lower promotion to the CO_2 photocatalytic reduction performance of g-C_3N_4.

Further investigations were carried out to find the reasons to why the binding energy of H_2CO_3 changes differently on K/g-C_3N_4 and Na/g-C_3N_4. One reason could be the different preferred positions of K^+ and Na^+ on the g-C_3N_4 sheet. As mentioned earlier, Na stays nearly in-plane with the g-C_3N_4 sheet while K is out of the pore. Therefore, it is easier for the H_2CO_3 to coordinate with K than Na. In another word, there is more steric hindrance for the interaction of H_2CO_3 with the Na/g-C_3N_4. The other reason could be the possibly different electron densities in the sheet with K and Na. Fig. 13 exhibits the charge density difference for Na/g-C_3N_4 and K/g-C_3N_4, which is obtained by subtraction the charge density of the separated species (K or Na and g-C_3N_4) from the charge density of the complex. Both K and Na are cationic with higher electron density on the sheet near the ions. The charge density differences of the sheets with either of the atoms are nearly identical, except in the charge depleted region around the alkali metal atom itself. A larger area is shown around K than around Na. That is, when K is present, there is a larger region where H_2CO_3 can be stabilized. In addition, little change in adsorption energy of H_2CO_3 on local minimum energy sites away from the K/Na ion is found, suggesting that the additional electrons in the unit cell of g-C_3N_4 won't influence the adsorption of H_2CO_3. It is only K^+ and Na^+ that are responsible for the enhanced stabilization of H_2CO_3.

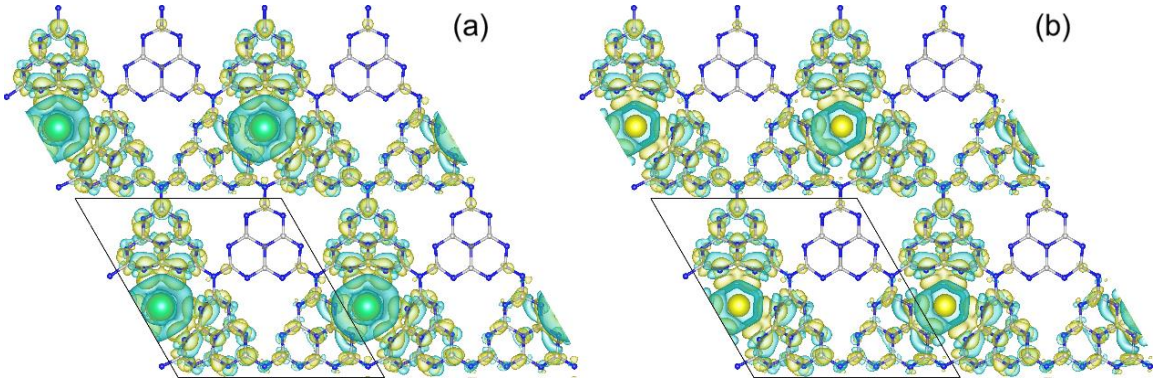

Fig. 13 Charge density differences with K (a) and Na (b) on g-C_3N_4. (Iso-level of 0.0008 e/bohr^3; Grey – Carbon atoms, blue – nitrogen atoms, green – potassium atoms and yellow – sodium atoms; Charge depletion in aqua and accumulation in yellow; Box shows the size of the super cell.)

For g-C_3N_4 samples synthesized by polymerization of a certain precursor, there are always residual hydrogens connected to the nitrogen due to incomplete condensation.[20]

Therefore, additionaly, we calculated the adsorption energy of H_2CO_3 on the g-C_3N_4 system containing hydrogen (Fig. 1b) and an enhanced adsorption was observed compared to the pure g-C_3N_4 sheet. The binding energy for H_2CO_3 on g-C_3N_4 with -NH is 1.08 eV and the molecule will sit in the pore with –NH groups. The increased binding energy is supposed to be originated from the hydrogen bonding between the adsorbate and the sheet.

When K and Na are added to the g-C_3N_4 sheet with some pores containing–NH groups while some not. It is found that the K and Na greatly prefer to bind to a pore that did not contain –NH. And the binding energies of alkali-metal atoms are larger on the pores of the pure sheet (K: 3.47 eV and Na: 3.64 eV) than on the pores adjacent to –NH bond in the –NH containing sheet (K: 3.20 eV and Na: 3.57 eV). This difference of binding energies at the two sites is higher with K (0.27 eV) than with Na (0.07 eV). Both metals, and especially K, would therefore prefer to sit on sections of the material that are far away from the pores containing –NH. In this light, the reduced promoting effect of KOH when excessive amount of KOH is decorated could also be explained by the fact that K selectively adsorbes on the pores without hydrogen and only as its concentration increases to a certain value would it also adsorbs to pores adjacent to –NH bonds and reduces the adsorption energy of the reaction intermediate, H_2CO_3, in the pore with the –NH bonds to 0.95 eV. In contrast, the adsorption of Na is less selective between pores adjacent to –NH groups and the pores on clean sheet, but it would also weaken the binding energy of H_2CO_3 in the hydrogen-containing material (from 1.03 eV to 0.94 eV). Therefore, it could be concluded that both the lower enhancement to the adsorption of H_2CO_3 on clean g-C_3N_4 and the poorer selectivity to favorable sitting sites contribute to the inferior promoting effect of NaOH on g-C_3N_4 for CO_2 photocatalytic reduction compared to KOH.

3.7 Deactivation of the catalyst

Deactivation of the photocatalytic reduction of CO_2 in the absence of a sacrificial agent is very common for various materials, including TiO_2, [6] Bi_2WO_6, [13] $ZnGeO_4$, [56] and g-C_3N_4 [52] etc., due to inhibited desorption of some intermediates and enhanced back reaction with the formation of oxygen. [6] The deactivation of g-C_3N_4 was also observed in this work. As presented in Fig. 14, the evolution rate of the products (CO, CH_4 and CH_3CHO) on pristine g-C_3N_4 (CN) was found to increase in the first hour and then gradually decrease due to the deactivation. Decorating KOH onto g-C_3N_4 as a strategy to enhance CO_2 reduction might be expected to exacerbate this problem due to possible conversion of KOH to $KHCO_3$ or K_2CO_3 during the reaction with a fast loss of its promoting effect. However, comparing the activity change of CN and 0.1K-CN as presented in Fig. 14, the drop of photocatalytic efficiency with 0.1KOH-CN is even slower than that with CN, suggesting that the chemical change of KOH on g-C_3N_4 could not be dramatic.

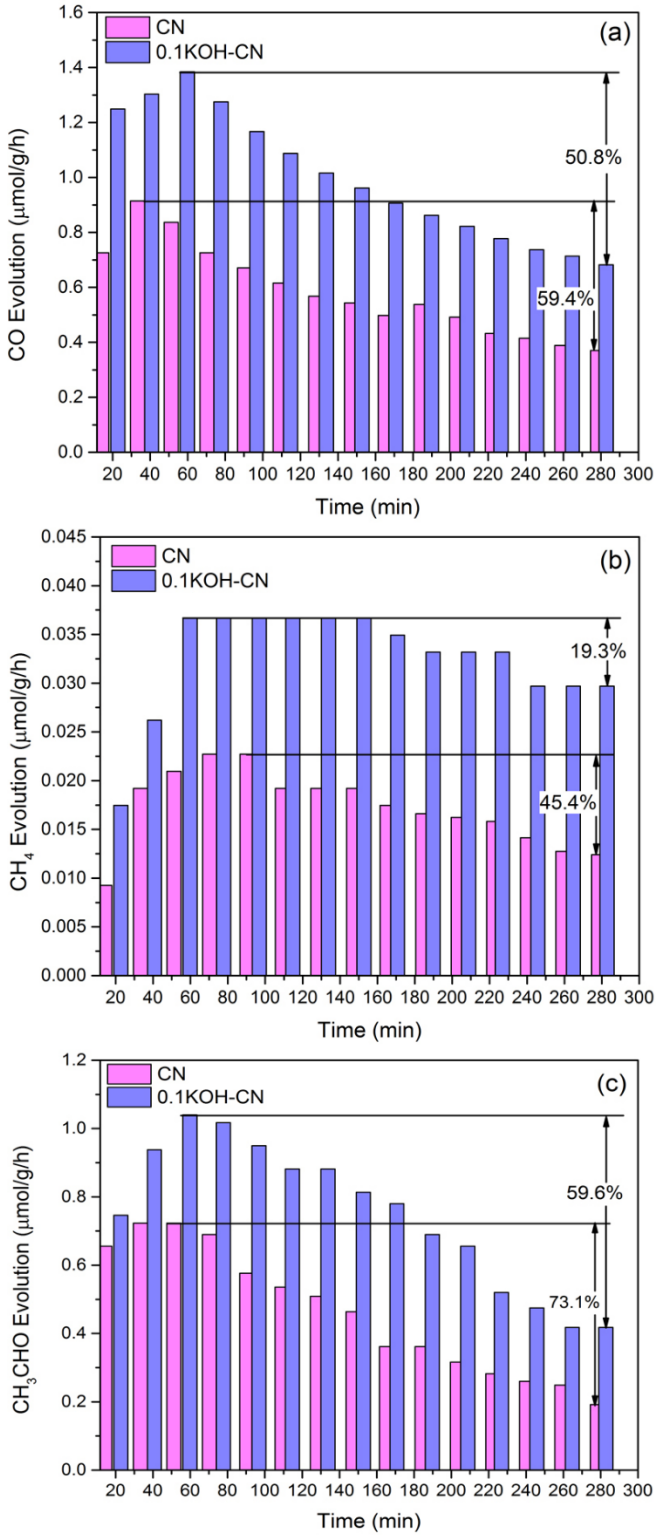

Fig. 14 Time-course evolutions of CO (a), CH_4 (b) and CH_3CHO (c) over CN and 0.1KOH-CN.

To analyze this further, DRIFTS experiments were carried out on 0.1KOH-CN. Using the clean 0.1KOH-CN surface treated with helium at 200 ˚C as a background, the in-situ DRIFT spectrum of 0.1KOH-CN after 60-min adsorption of CO_2 and H_2O gas mixture and a further

30-min He purging is presented in Fig. 15 along with the spectrum of the adsorbed surface after 120-min light irradiation. After the adsorption of CO_2 and H_2O, beside the adsorption peak of H_2O at 1650 cm^{-1}, absorption peaks of HCO_3^- and CO_3^{2-} are apparent at 1598, 1306 cm^- and 1699, 1544, 1352 cm^{-1}, respectively, [21, 40] suggesting KOH has been partially converted to $KHCO_3$ and K_2CO_3 before the photocatalytic reactions. After 120-min irradiation, the absorbance of HCO_3^- shows a certain decrease whereas the peaks due to presence of CO_3^{2-} remains or increases. And new absorptions of formate (-$HCOO^-$) (1518, 1416 cm^{-1}) and formaldehyde (-CHO) (1682, 1460, 1397 cm^{-1}) from the intermediates in CO_2 photocatalytic reduction [21, 57, 58] appear. Note, the CO_3^{2-} peaks that show increase in intensity are close to these new peaks, so their increase could be at least partially attributed to overlap with the new peaks. Overall, the total amount of HCO_3^- and CO_3^{2-} does not show much difference before and after irradiation, validating the robustness of the effect of KOH on g-C_3N_4.

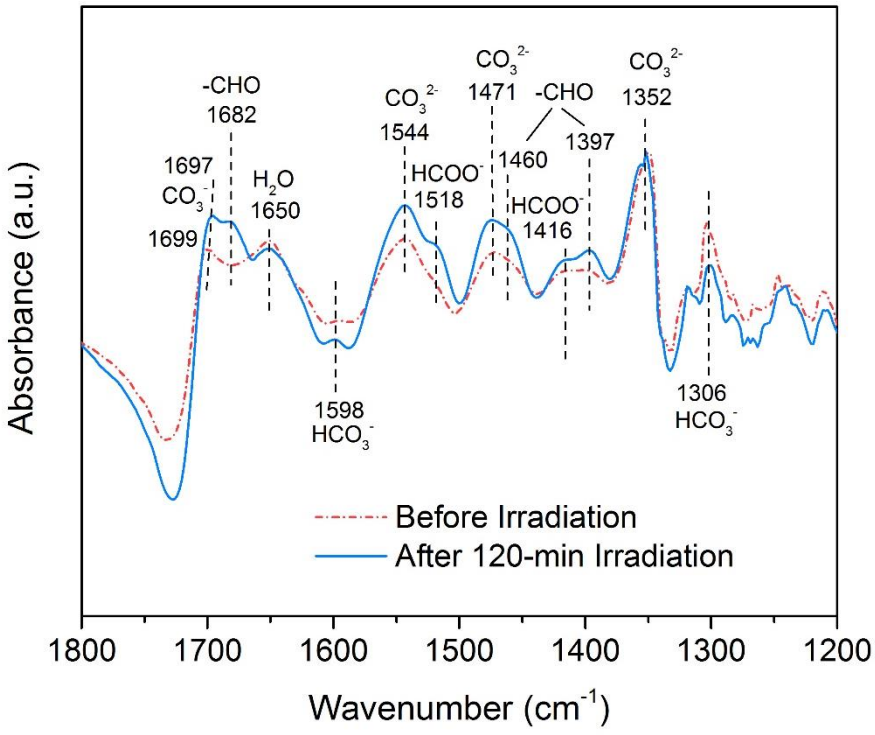

Fig. 15 In-situ DRIFT spectra of 0.1KOH-CN with adsorbed forms of H_2O and CO_2: before irradiation and after 120-min light irradiation.

4. Conclusion

In this work, we reported the remarkably improved photocatalytic activity of CO_2 reduction over KOH-decorated g-C_3N_4 compared to pristine g-C_3N_4. With the formation of a thin layer of alkaline electrolyte due to its high deliquescence, OH^- functioning as a hole

acceptor, a certain amount of KOH kept and facilitated the formation and consumption cycle of H_2CO_3 which is assumed to be the main species involved in the alkali-promoted photocatalytic reduction process. In addition, it was found that the promotion effect of KOH was much more obvious than NaOH. Though DFT calculation, the reasons turned out to contain that (1) while both K^+ and Na^+ were found to be able to enhance the binding of H_2CO_3 on clean g-C_3N_4 pores, the influence of K^+ is much stronger; and (2) for commonly sysnthesize g-C_3N_4 with $–NH_x$, K^+/Na^+ located adjacent to the pore with -NH would impair the adsorption of H_2CO_3 but K^+ showed a higher selectivity to staying at the sites far away from the -NH-containing pores. Furthermore, the robustness of the effect of KOH on g-C_3N_4 during the photocatalytic process was verified. The findings not only provide insights into the understanding the first step of CO_2 photocatalytic reduction (CO_2 adsorption) on alkali-modified photocatalysts, but also should inspire the development of efficient photocatalysts for CO_2 photocatalytic reduction.

Acknowledgment

We acknowledge the financial supports of the Natural Science Foundation of Zhejiang Province (No. Z5100116), National Natural Science Foundation of China (No. 51578488), Changjiang Scholar Program of Chinese Ministry of Education (China, 2009). We thank the Australian Research Council for support of this project through the DP and LIEF programs. This research was undertaken with the assistance of resources provided at the NCI National Facility systems at the Australian National University through the National Computational Merit Allocation Scheme supported by the Australian Government with support from the Queensland Cyber Infrastructure Foundation (QCIF) and the University of Queensland Research Computing Centre. J.M.T.A.F. thanks the University of Queensland for the UQI scholarships supporting her Ph.D.

Reference

[1] T. Inoue, A. Fujishima, S. Konishi, K. Honda, Nature 277 (1979) 637-638.

[2] S.N. Habisreutinger, L. Schmidt-Mende, J.K. Stolarczyk, Angew. Chem. Int. Ed. 52 (2013) 7372-7408.

[3] M. Mikkelsen, M. Jorgensen, F.C. Krebs, Energy Environ. Sci. 3 (2010) 43-81.

[4] S. Navalón, A. Dhakshinamoorthy, M. Álvaro, H. Garcia, ChemSusChem 6 (2013) 562-577.

[5] M. Tahir, N.S. Amin, Energy Convers. Manage. 76 (2013) 194-214.

[6] W. Tu, Y. Zhou, Z. Zou, Adv. Mater. 26 (2014) 4607-4626.

[7] S. Ye, R. Wang, M.-Z. Wu, Y.-P. Yuan, Appl. Surf. Sci. 358 (2015) 15-27.

[8] K. Li, B.S. Peng, T.Y. Peng, ACS Catal. 6 (2016) 7485-7527.

[9] A.D. Handoko, J. Tang, Int. J. Hydrogen Energy 38 (2013) 13017-13022.

[10] Y. Wang, F. Wang, Y. Chen, D. Zhang, B. Li, S. Kang, X. Li, L. Cui, Appl. Catal., B 147 (2014) 602-609.

[11] P. Li, Y. Zhou, Z. Zhao, Q. Xu, X. Wang, M. Xiao, Z. Zou, J. Am. Chem. Soc. 137 (2015) 9547-9550.

[12] K. Li, A.D. Handoko, M. Khraisheh, J. Tang, Nanoscale 6 (2014) 9767-9773.

[13] Z. Sun, Z. Yang, H. Liu, H. Wang, Z. Wu, Appl. Surf. Sci. 315 (2014) 360-367.

[14] T. Baran, S. Wojtyła, A. Dibenedetto, M. Aresta, W. Macyk, Appl. Catal., B 178 (2015) 170-176.

[15] J. Chen, S. Qin, G. Song, T. Xiang, F. Xin, X. Yin, Dalton Trans. 42 (2013) 15133-15138.

[16] H.-C. Hsu, I. Shown, H.-Y. Wei, Y.-C. Chang, H.-Y. Du, Y.-G. Lin, C.-A. Tseng, C.-H. Wang, L.-C. Chen, Y.-C. Lin, K.-H. Chen, Nanoscale 5 (2013) 262-268.

[17] H. Wang, Z. Sun, Q. Li, Q. Tang, Z. Wu, J. CO2 Util. 14 (2016) 143-151.

[18] S. Cao, J. Low, J. Yu, M. Jaroniec, Adv. Mater. 27 (2015) 2150-2176.

[19] A. Thomas, A. Fischer, F. Goettmann, M. Antonietti, J.-O. Muller, R. Schlogl, J.M. Carlsson, J. Mater. Chem. 18 (2008) 4893-4908.

[20] W.-J. Ong, L.-L. Tan, Y.H. Ng, S.-T. Yong, S.-P. Chai, Chem. Rev. 116 (2016) 7159-7329.

[21] P. Xia, B. Zhu, J. Yu, S. Cao, M. Jaroniec, J. Mater. Chem. A 5 (2017) 3230-3238.

[22] Z. Zhao, Y. Sun, F. Dong, Nanoscale 7 (2015) 15-37.

[23] N. Tian, H. Huang, C. Liu, F. Dong, T. Zhang, X. Du, S. Yu, Y. Zhang, J. Mater. Chem. A 3 (2015) 17120-17129.

[24] Q. Zhang, H. Wang, S. Hu, G. Lu, J. Bai, X. Kang, D. Liu, J. Gui, RSC Advances 5 (2015) 42736-42743.

[25] B. Lin, G. Yang, B. Yang, Y. Zhao, Appl. Catal., B 198 (2016) 276-285.

[26] S.-W. Cao, X.-F. Liu, Y.-P. Yuan, Z.-Y. Zhang, Y.-S. Liao, J. Fang, S.C.J. Loo, T.C. Sum, C. Xue, Appl. Catal., B 147 (2014) 940-946.

[27] H. Shi, G. Chen, C. Zhang, Z. Zou, ACS Catal. 4 (2014) 3637-3643.

[28] M. Li, L. Zhang, X. Fan, Y. Zhou, M. Wu, J. Shi, J. Mater. Chem. A 3 (2015) 5189-5196.

[29] Y. HUANG, M. FU, T. HE, Acta Phys. Chim. Sin. 31 (2015) 1145-1152.

[30] Y. He, L. Zhang, B. Teng, M. Fan, Environ. Sci. Technol. 49 (2015) 649-656.

[31] J.-C. Wang, H.-C. Yao, Z.-Y. Fan, L. Zhang, J.-S. Wang, S.-Q. Zang, Z.-J. Li, ACS Appl. Mater. Interfaces 8 (2016) 3765-3775.

[32] M. Li, L. Zhang, X. Fan, M. Wu, M. Wang, R. Cheng, L. Zhang, H. Yao, J. Shi, Appl. Catal., B 201 (2017) 629-635.

[33] Y. Wang, R. Shi, J. Lin, Y. Zhu, Energy Environ. Sci. 4 (2011) 2922-2929.

[34] W. Yu, D. Xu, T. Peng, J. Mater. Chem. A 3 (2015) 19936-19947.

[35] M. Li, L. Zhang, M. Wu, Y. Du, X. Fan, M. Wang, L. Zhang, Q. Kong, J. Shi, Nano Energy 19 (2016) 145-155.

[36] H. Li, S. Gan, H. Wang, D. Han, L. Niu, Adv. Mater. 27 (2015) 6906-6913.

[37] Q. Huang, J. Yu, S. Cao, C. Cui, B. Cheng, Appl. Surf. Sci. 358 (2015) 350-355.

[38] L. Shi, T. Wang, H. Zhang, K. Chang, J. Ye, Advanced Functional Materials 25 (2015) 5360-5367.

[39] L. Liu, C. Zhao, H. Zhao, D. Pitts, Y. Li, Chem Commun (Camb) 49 (2013) 3664-3666.

[40] L. Liu, C. Zhao, D. Pitts, H. Zhao, Y. Li, Cata. Sci. & Tech. 4 (2014) 1539-1546.

[41] S. Xie, Y. Wang, Q. Zhang, W. Fan, W. Deng, Y. Wang, Chem Commun (Camb) 49 (2013) 2451-2453.

[42] S. Xie, Y. Wang, Q. Zhang, W. Deng, Y. Wang, ACS Catal. 4 (2014) 3644-3653.

[43] X. Meng, S. Ouyang, T. Kako, P. Li, Q. Yu, T. Wang, J. Ye, Chem. Commun. 50 (2014) 11517-11519.

[44] G. Kresse, J. Furthmüller, Physical Review B 54 (1996) 11169-11186.

[45] J.P. Perdew, K. Burke, M. Ernzerhof, Phys. Rev. Lett. 77 (1996) 3865-3868.

[46] S. Grimme, J. Comput. Chem. 27 (2006) 1787-1799.

[47] M. Hankel, D. Ye, L. Wang, D.J. Searles, J. Phys. Chem. C 119 (2015) 21921-21927.

[48] S.C. Yan, Z.S. Li, Z.G. Zou, Langmuir 25 (2009) 10397-10401.

[49] F. Dong, L. Wu, Y. Sun, M. Fu, Z. Wu, S.C. Lee, J. Mater. Chem. 21 (2011) 15171-15174.

[50] J. Liu, T. Zhang, Z. Wang, G. Dawson, W. Chen, J. Mater. Chem. 21 (2011) 14398-14401.

[51] Y. Zhang, J. Liu, G. Wu, W. Chen, Nanoscale 4 (2012) 5300-5303.

[52] J. Yu, K. Wang, W. Xiao, B. Cheng, Phys. Chem. Chem. Phys. 16 (2014) 11492-11501.

[53] S. Sato, J.M. White, J. Catal. 69 (1981) 128-139.

[54] B. Kumar, M. Llorente, J. Froehlich, T. Dang, A. Sathrum, C.P. Kubiak, Annu. Rev. Phys. Chem. 63 (2012) 541-569.

[55] H. Zhong, K. Fujii, Y. Nakano, F. Jin, J. Phys. Chem. C 119 (2015) 55-61.

[56] Q.Z. Liu, Y. Tian, Z. P. Chen, X. Y. Gao, J. Zou, Z. G., J. Mater. Chem. 22 (2012) 2033-2038.

[57] S.E. Collins, M.A. Baltanás, A.L. Bonivardi, J. Catal. 226 (2004) 410-421.

[58] J. Araña, J.M. Doña-Rodríguez, C.G.i. Cabo, O. González-Díaz, J.A. Herrera-Melián, J. Pérez-Peña, Appl. Catal., B 53 (2004) 221-232.

Figure Caption

Figr-1

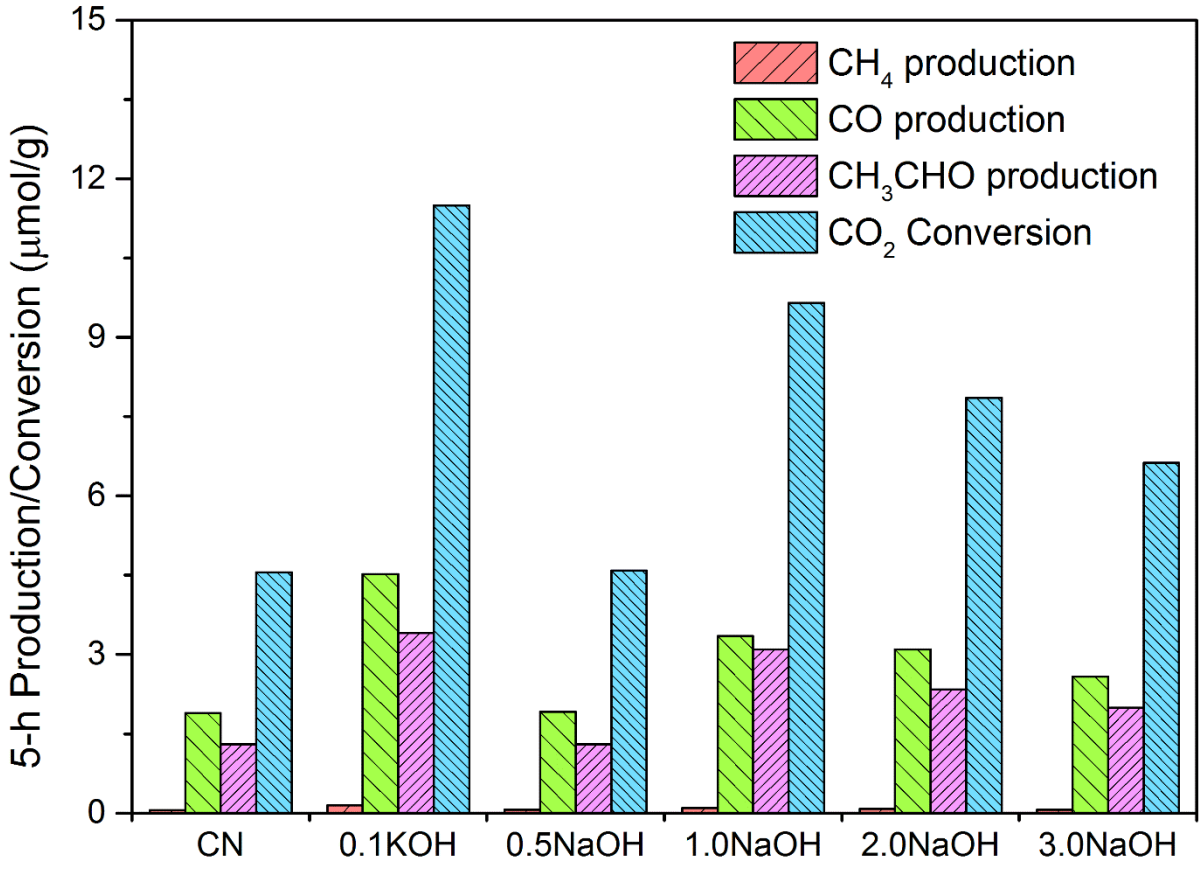

Figr-2

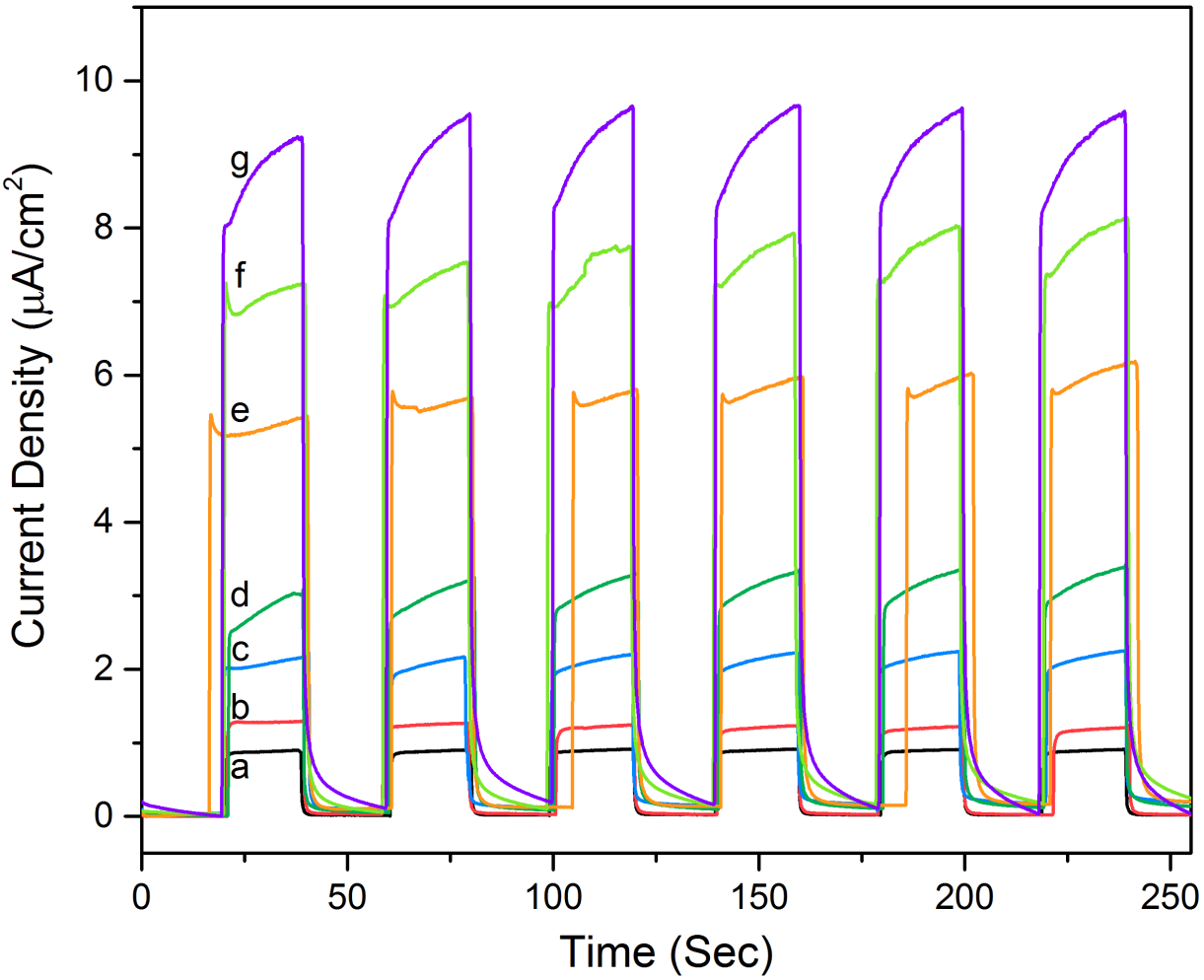

Figr-3

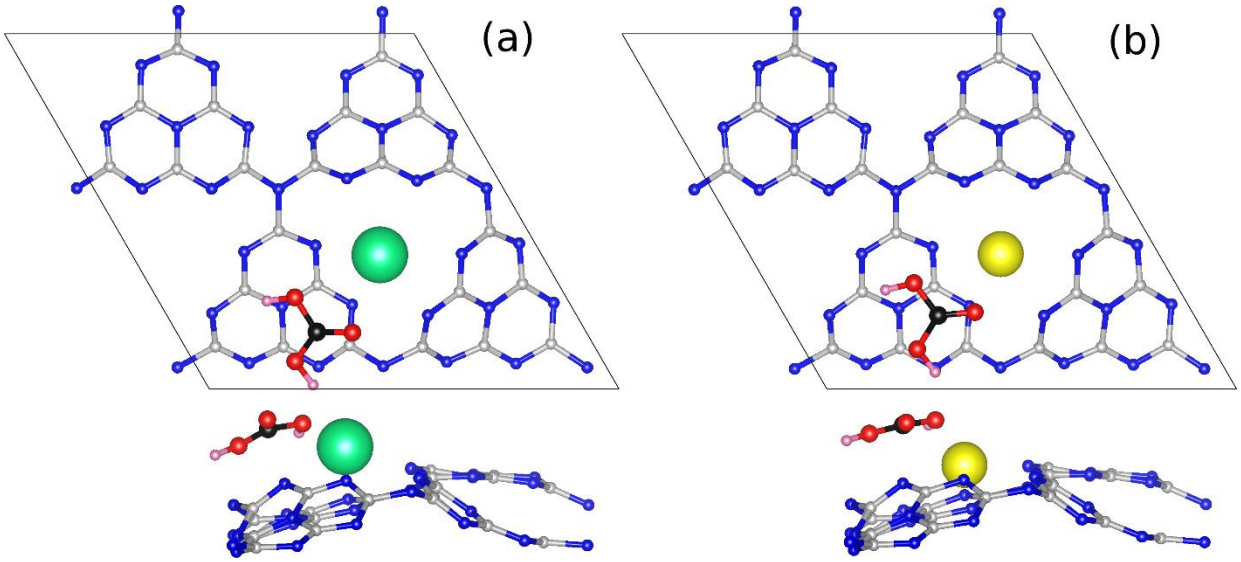

Figr-4

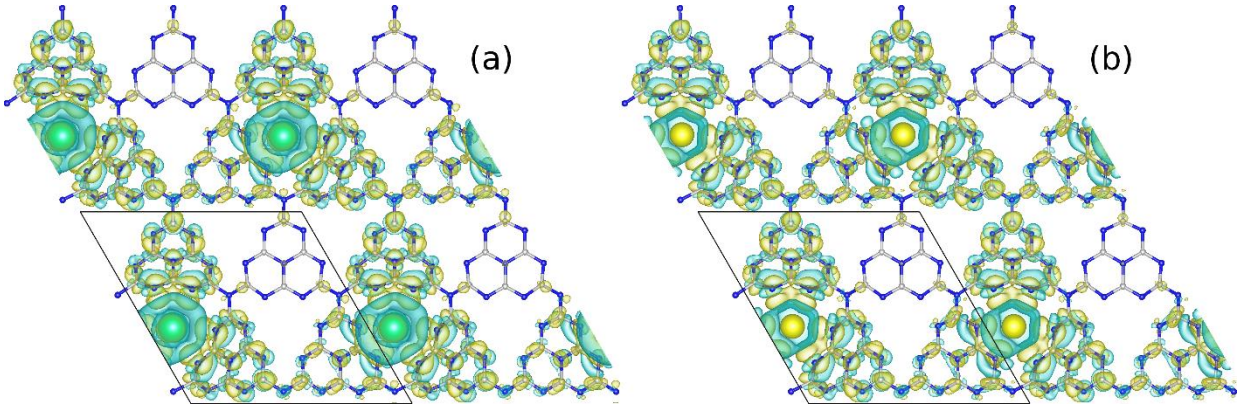

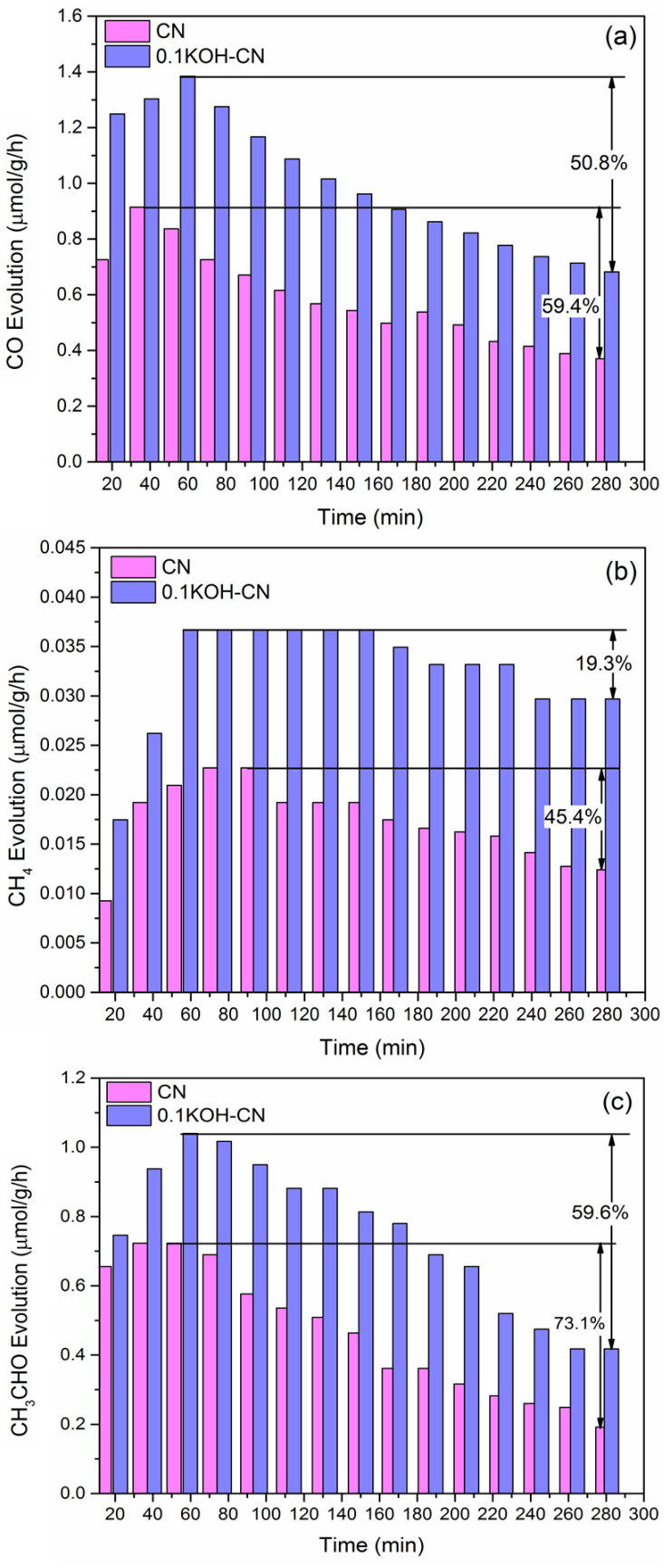

Figr-5

Figr-6

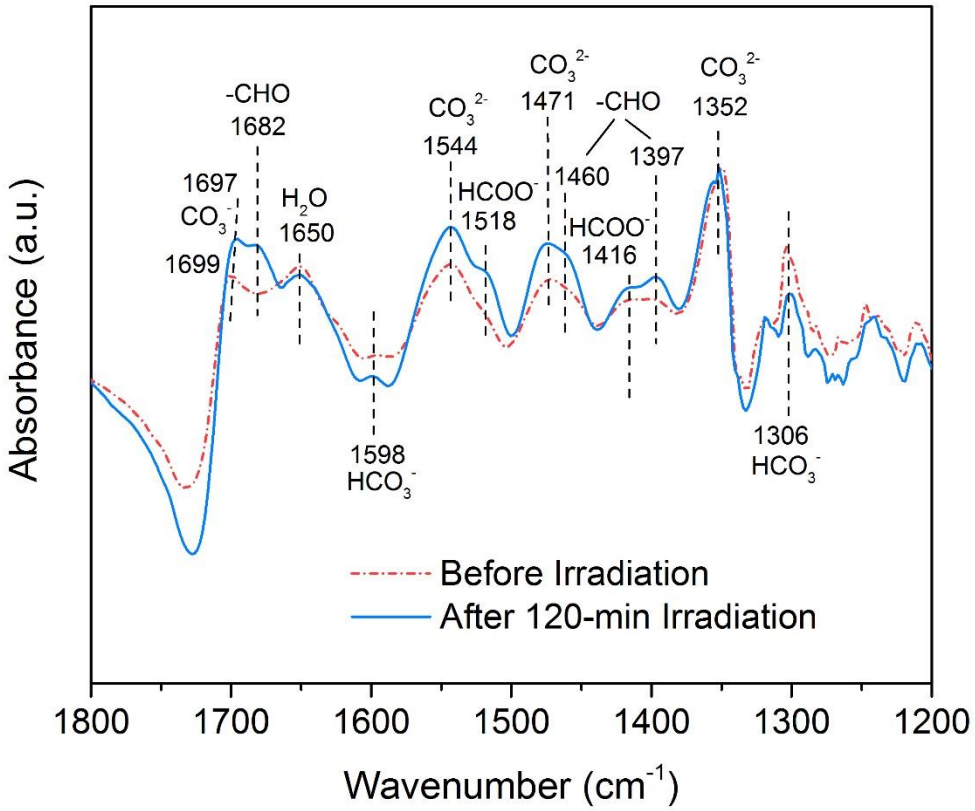

Figr-7

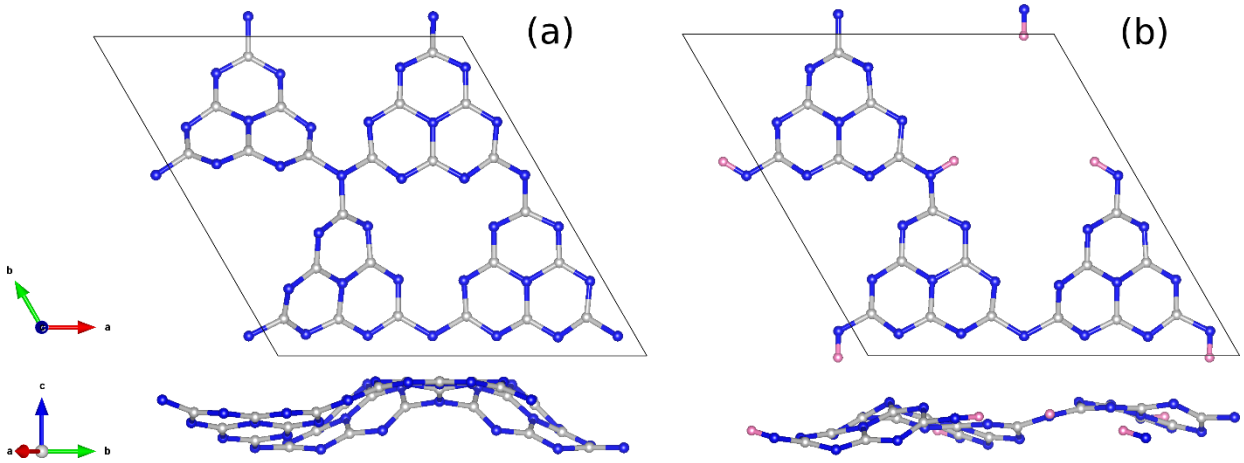

Figr-8

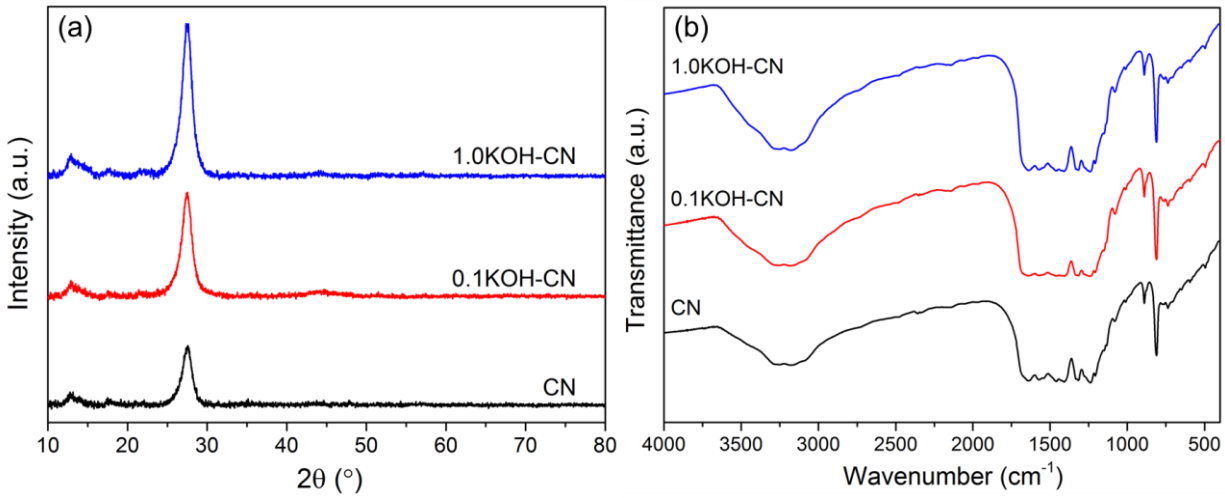

Figr-9

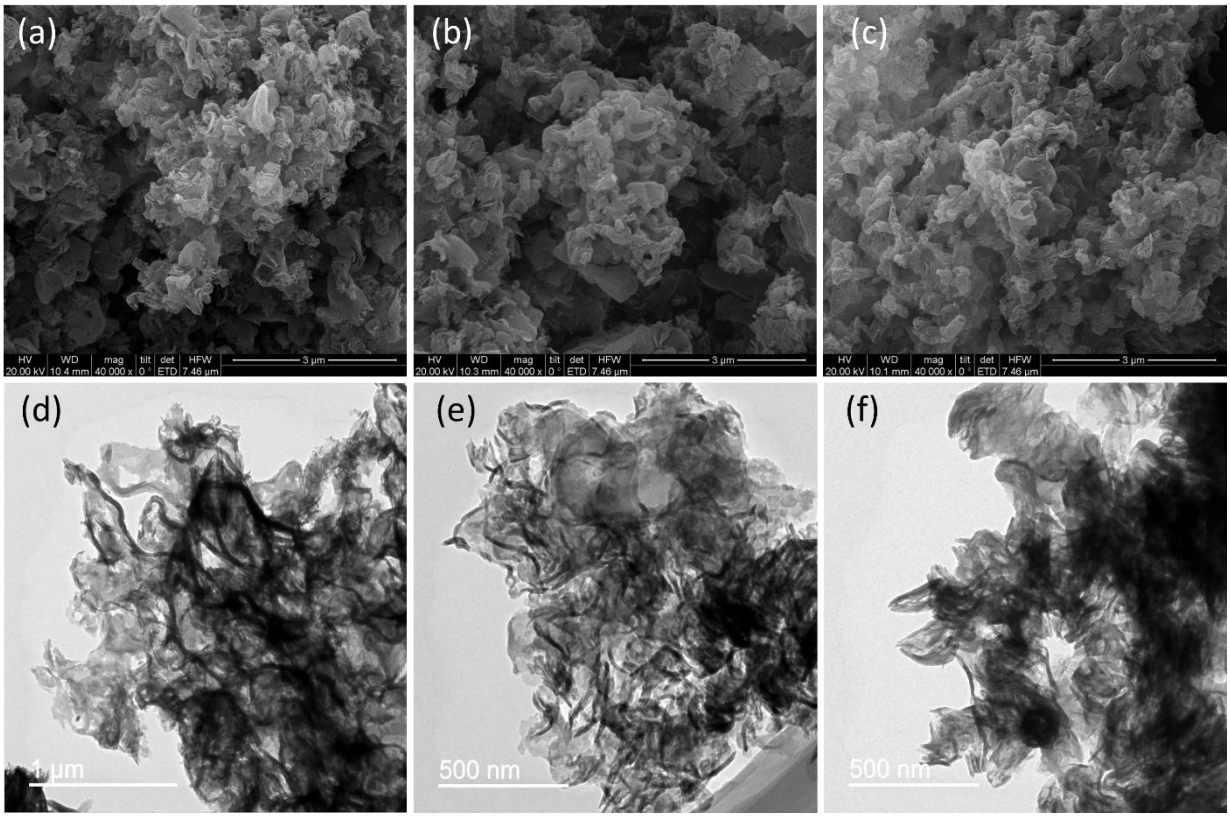

Figr-10

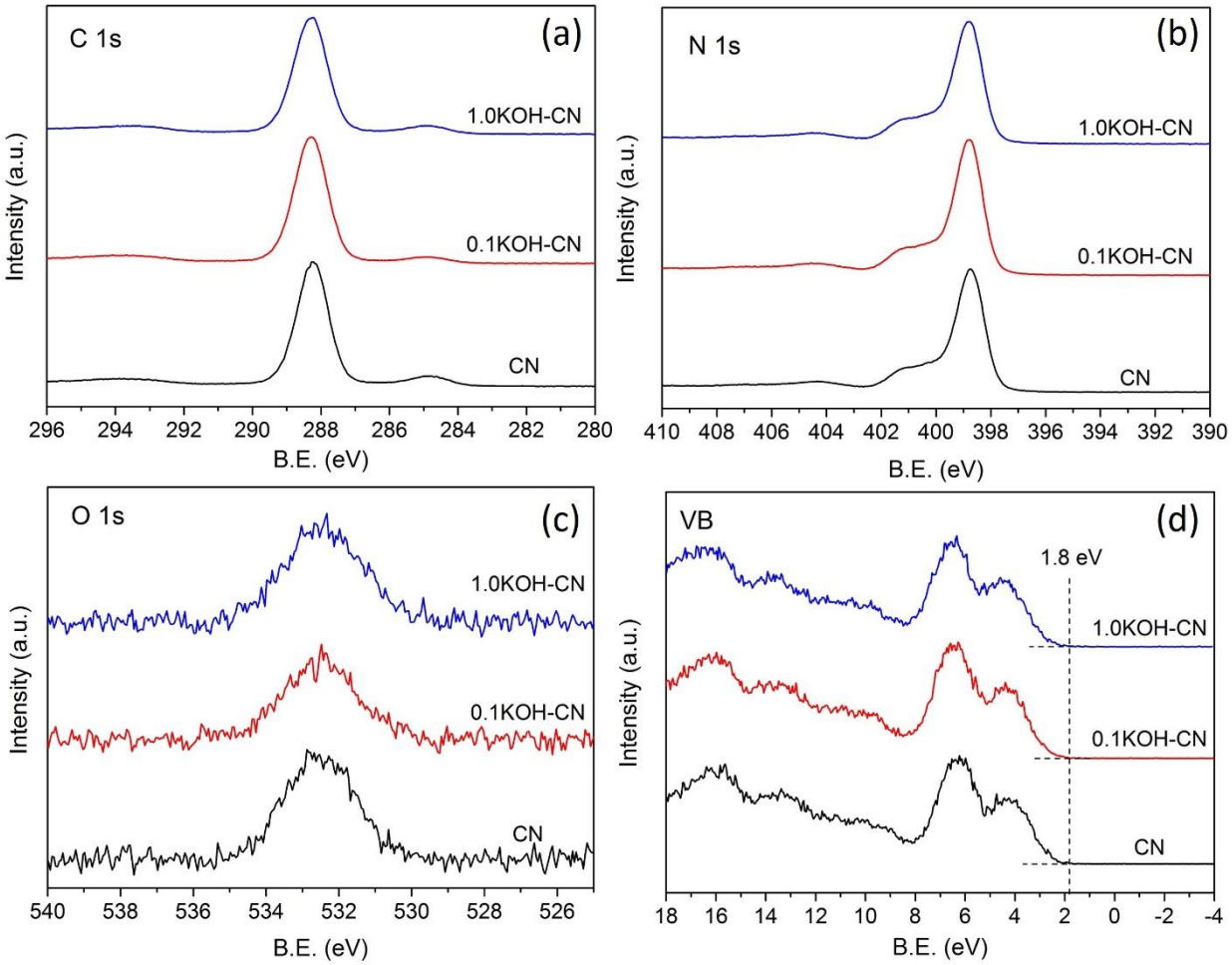

Figr-11

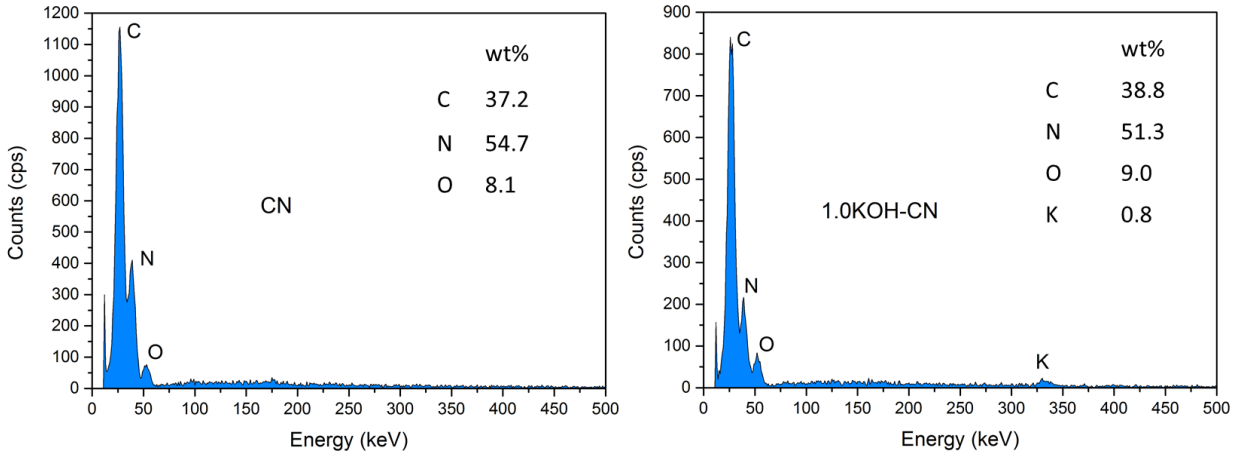

Figr-12

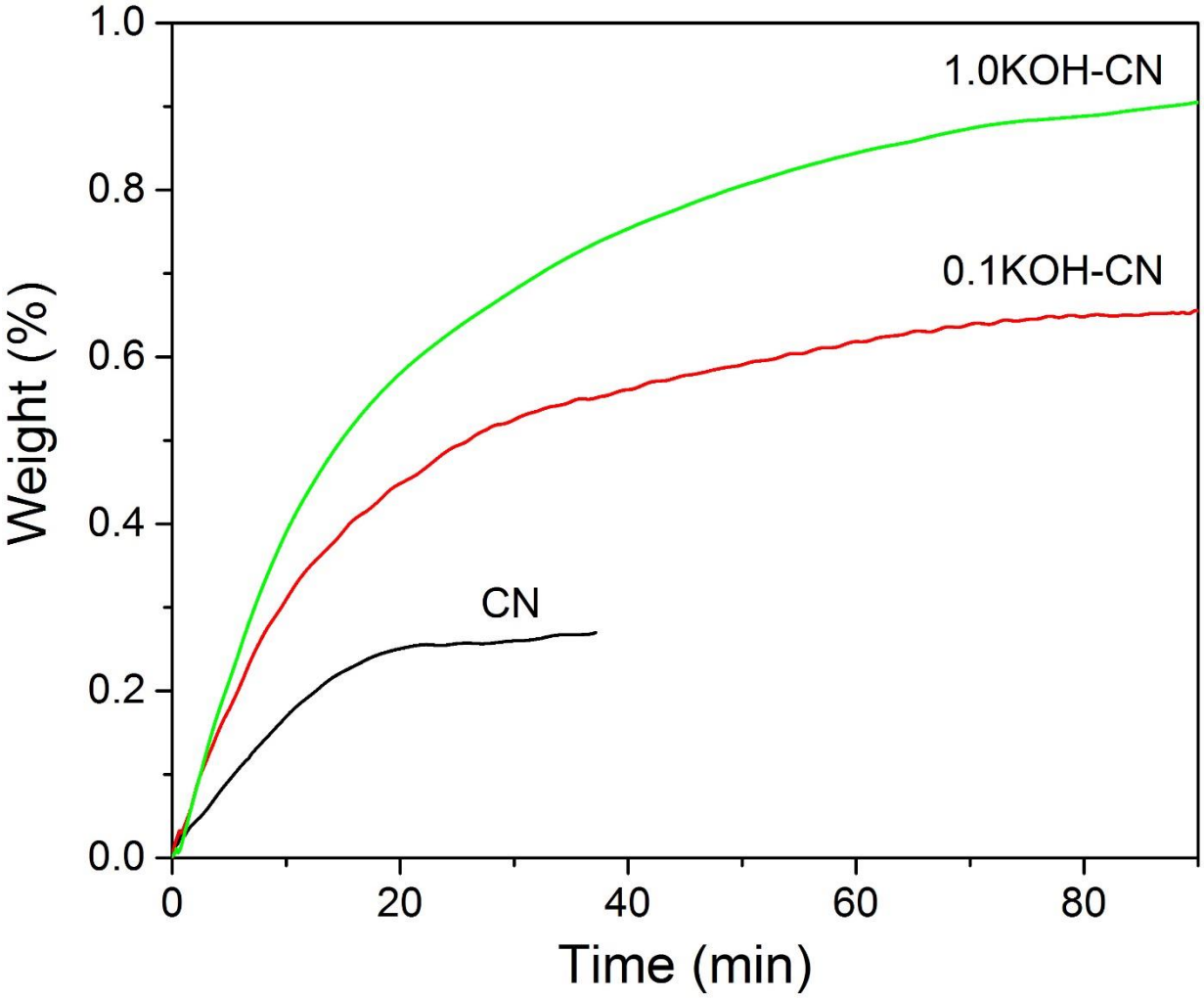

Figr-13

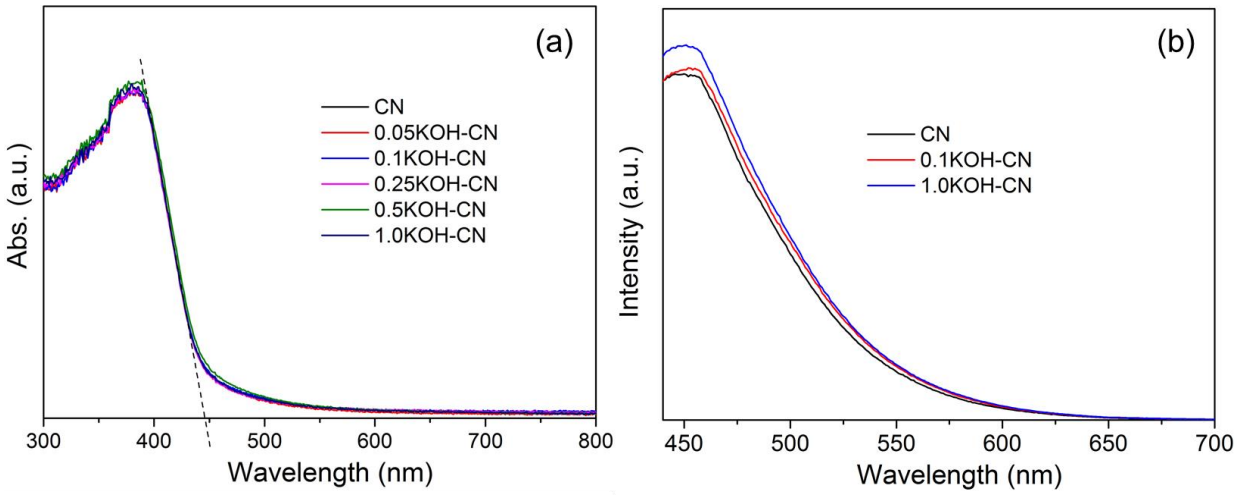

Figr-14

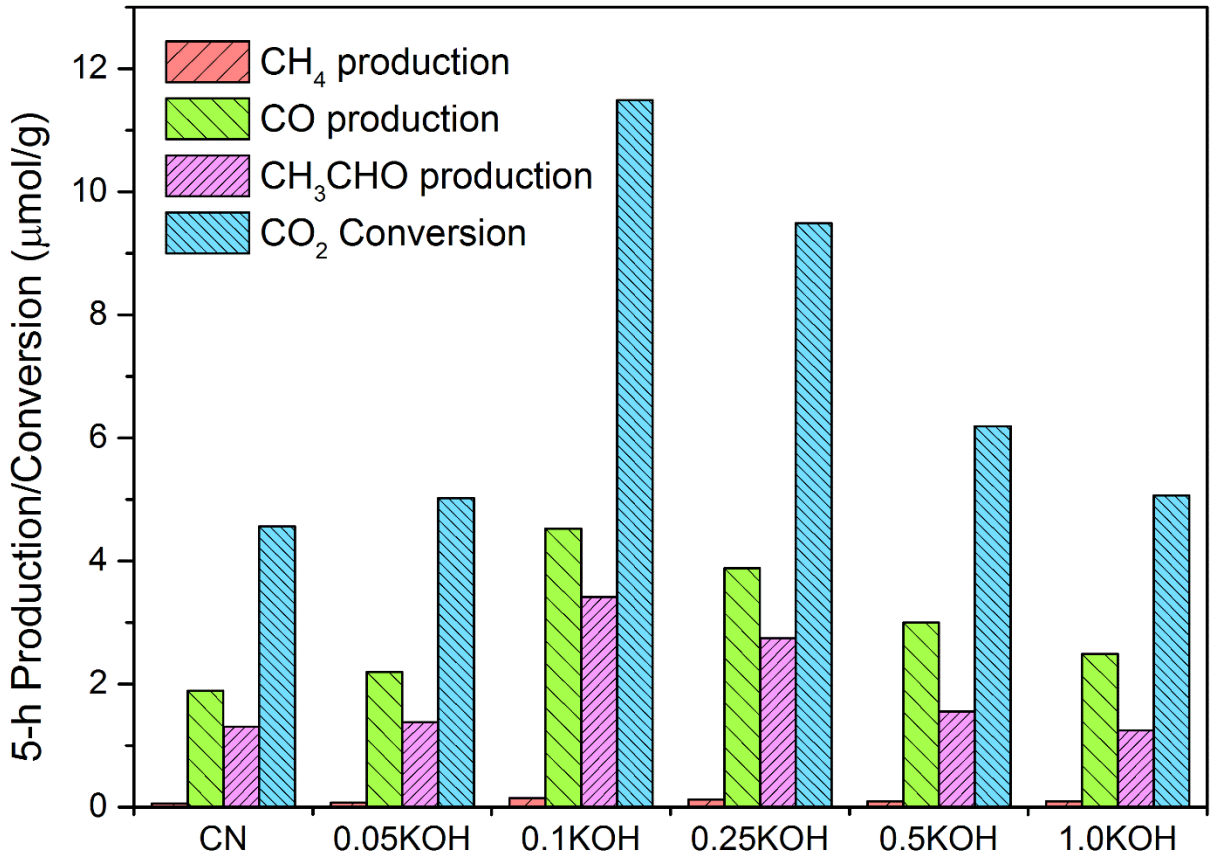

Figr-15

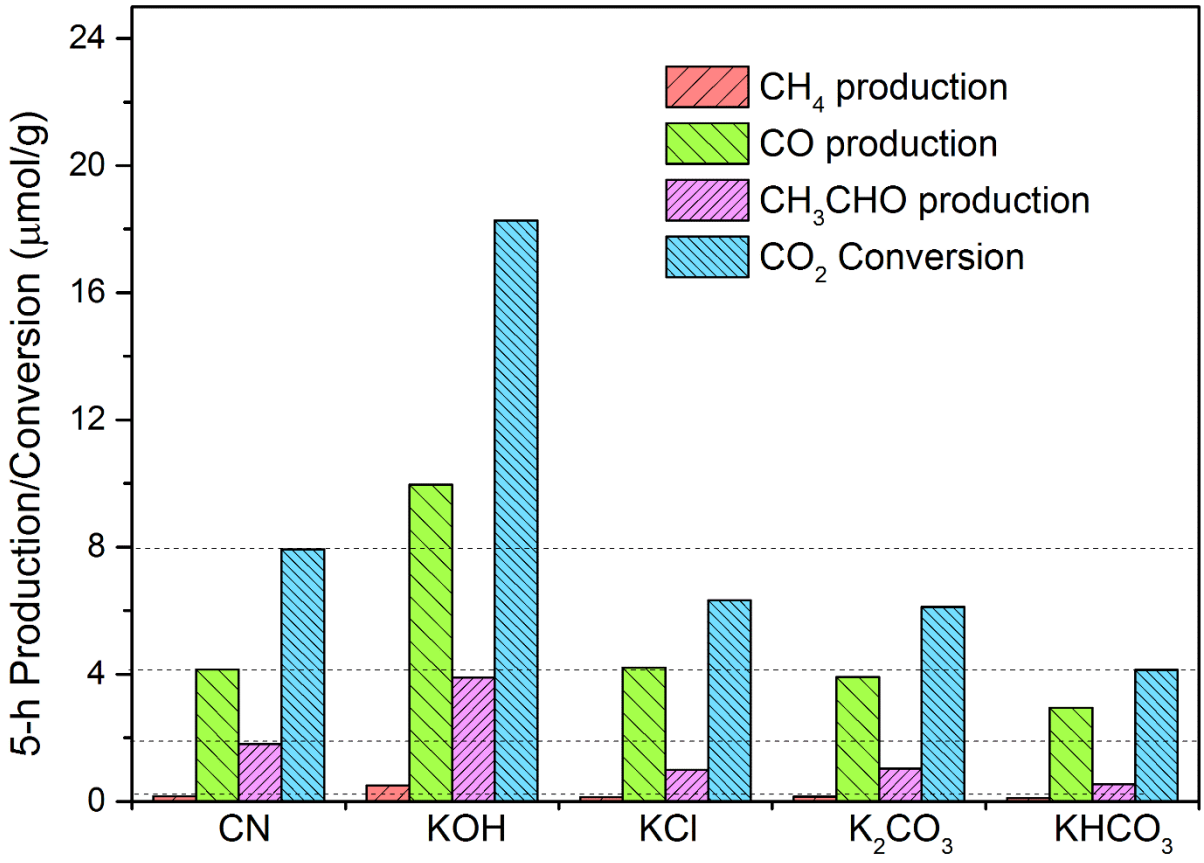

Table 1. BET surface areas of g-C_3N_4 and KOH decorated g-C_3N_4 samples

Sample	CN	0.05KOH-CN	0.1KOH-CN	0.25KOH-CN	0.5KOH-CN	1.0KOH-CN
BET surface area (m^2/g)	61.9	61.6	62.4	59.0	62.2	59.1